Author Manuscript

Mutations in *VPS13D* lead to a new recessive ataxia with spasticity and mitochondrial defects

RUNNING TITLE: VPS13D in ataxia/spastic paraplegia

Eunju Seong[1], PhD, Ryan Insolera[2], PhD, Marija Dulovic[3], PhD, Erik-Jan Kamsteeg[4], PhD, Joanne Trinh[3], PhD, Norbert Brüggemann[5], MD, Erin Sandford[1], PhD, Sheng Li[13], PhD, Ayse Bilge Ozel[6], PhD, Jun Z. Li[6,7], PhD, Tamison Jewett[8], MD, Anneke J.A. Kievit[9], MD PhD, Alexander Münchau[3], MD, Vikram Shakkottai[10], MD PhD, Christine Klein[3], MD, Catherine Collins[2], PhD, Katja Lohmann[3*], PhD, Bart P. van de Warrenburg[11*], MD PhD, Margit Burmeister[1,6,7,12*], PhD

Affiliations

[1]Molecular & Behavioral Neuroscience Institute, University of Michigan, Ann Arbor, MI 48109, USA.

[2]Department of Molecular, Cellular, and Developmental Biology, University of Michigan, Ann Arbor, MI 48109, USA.

[3]Institute of Neurogenetics, University of Lübeck, Germany

[4]Department of Human Genetics, Radboud University Medical Centre, Nijmegen, The Netherlands

[5]Department of Neurology, University of Lübeck, Germany

[6]Department of Human Genetics, University of Michigan, Ann Arbor, MI 48109, USA.

[7]Department of Computational Medicine & Bioinformatics, University of Michigan, Ann Arbor, MI 48109, USA.

[8]Department of Pediatrics, Section on Medical Genetics, Wake Forest School of Medicine, Winston-Salem, North Carolina, USA.

[9]Department of Clinical Genetics, Erasmus MC, Rotterdam, the Netherlands

[10]Departments of Neurology and of Molecular and Integrative Physiology, University of Michigan, Ann Arbor, MI 48109, USA

This is the author manuscript accepted for publication and has undergone full peer review but has not been through the copyediting, typesetting, pagination and proofreading process, which may lead to differences between this version and the Version of record. Please cite this article as doi:10.1002/ana.25220.

This article is protected by copyright. All rights reserved.

[11]Department of Neurology, Donders Institute for Brain, Cognition and Behaviour, Radboud University Medical Center, Nijmegen, The Netherlands

[12]Department of Psychiatry, University of Michigan, Ann Arbor, MI 48109, USA.

[13]Present Address: Bio-X Center, Shanghai Jiao Tong University, China.

*Corresponding authors:

Margit Burmeister
Molecular & Behavioral Neuroscience Institute
University of Michigan
5061 BSRB, 109 Zina Pitcher Place
Ann Arbor MI 48109-2200
+1 734 647 2186
margit@umich.edu

Bart van de Warrenburg
Department of Neurology 935
Donders Institute for Brain, Cognition and Behaviour,
Radboud University Medical Center
P.O. Box 9101,
6500 HB, Nijmegen, The Netherlands
+31-24-3613396
Bart.vandeWarrenburg@radboudumc.nl

Katja Lohmann
Institute for Neurogenetics
University of Lübeck
Maria-Goeppert-Straße 1
23562 Lübeck, Germany
+49 451 3101 8209
katja.lohmann@neuro.uni-luebeck.de

Author Manuscript

This article is protected by copyright. All rights reserved.

Author Manuscript

Abstract:

Objective: To identify novel causes of recessive ataxias, including spinocerebellar ataxia with saccadic intrusions, spastic ataxias and spastic paraplegia.

Methods: In an international collaboration, we independently performed exome sequencing in seven families with recessive ataxia and/or spastic paraplegia. To evaluate the role of *VPS13D* mutations, we evaluated a *Drosophila* knock-out model and investigated mitochondrial function in patient-derived fibroblast cultures.

Results: Exome sequencing identified compound heterozygous mutations in *VPS13D* on chromosome 1p36 in all seven families. This included a large family with 5 affected siblings with spinocerebellar ataxia with saccadic intrusions (*SCASI*), or spinocerebellar ataxia, recessive, type 4, *SCAR4.* Linkage to chromosome 1p36 was found in this family with a LOD score of 3.1. The phenotypic spectrum in our 12 patients was broad. Although most presented with ataxia, additional or predominant spasticity was present in 5 patients. Disease onset ranged from infancy to 39 years, and symptoms were slowly progressive and included loss of independent ambulation in 5. All but two patients carried a loss-of-function (nonsense or splice site) mutation on one and a missense mutation on the other allele. Knock-down or removal of *Vps13D* in *Drosophila* neurons led to changes in mitochondrial morphology and impairment in mitochondrial distribution along axons. Patient fibroblasts showed altered morphology and functionality including reduced energy production.

Interpretation: Our study demonstrates that compound heterozygous mutations in *VPS13D* cause movement disorders along the ataxia-spasticity spectrum, making *VPS13D* the fourth VPS13 paralog involved in neurological disorders.

This article is protected by copyright. All rights reserved.

Author Manuscript

Introduction

Ataxia is a symptom of over 400 syndromic neurological conditions or can be the sole symptom of >80 recessively, dominantly, or X-linked inherited genetically defined conditions.[1-3] Recessive forms of ataxia are clinically and genetically more heterogeneous than dominant ataxias. Only in a minor fraction (~20%) of idiopathic or suspected recessive ataxia cases can a mutation in a known ataxia gene be identified,[4] suggesting that much of the genetic heterogeneity still remains to be discovered. In addition to heterogeneity, there is also pleiotropy, as the spectrum of ataxias also includes clinical and molecular overlap with, for example, the spastic paraplegias.[5]

Here, we report 12 patients from 7 families with compound heterozygous mutations in *VPS13D*. All patients > 2 years old have ataxia and/or spasticity, while the one 2 year old patient shows developmental delay, hypotonia, and is nonambulatory (Table 1). The phenotype in one of these families, comprising 5 patients (Figure 1), has previously been described in detail.[6, 7] Briefly, patients in this family demonstrated early adult-onset cerebellar ataxia with neuropathy and pyramidal signs, as well as striking saccadic intrusions, hence initially referred to as spinocerebellar ataxia with saccadic intrusion (*SCASI),*[6] later renamed spinocerebellar ataxia, recessive 4 (*SCAR4)*. Analysis of a *Drosophila* knock-out model and patient-derived fibroblasts suggests that mutations in this new ataxia/spasticity gene impact on mitochondrial structure and function.

This article is protected by copyright. All rights reserved.

Author Manuscript

Methods:

Patients:

Patients were identified in five different centers with a focus on movement disorders located in Case Western Reserve University (Ohio, US and genetically analyzed in Ann Arbor [Michigan, USA, UM1]), Nijmegen and Rotterdam (The Netherlands, NIJ1-4), Lübeck (Germany, LUB1) and Winston-Salem (North Carolina, USA, WF1). Diagnostic testing (including gene panel analysis of known ataxia/spasticity genes) did not reveal a molecular diagnosis in these cases. All patients and relatives gave written informed consent to participate in diagnostic or research studies that were approved by the respective local IRBs (IRBMED University of Michigan, University of Lübeck ethics review panel, or to local (NIJ and Rotterdam) or commercial (WF1, GeneDx, Gaithersburg, MD) clinical exome sequencing (NIJ and WF1). Formation of this collaboration was facilitated by publication of grants funded by the National Ataxia Foundation and by "GeneMatcher".[8]

Genetic studies: Linkage analysis and exome sequencing

In Family UM1, linkage analysis was performed with DNA from all 5 affecteds, the mother and 7 unaffected siblings using the Infinium HumanLinkage-24 Beadchip kit (6000 markers, Illumina, WG-32-140), followed by parametric fully penetrant recessive model analysis in Merlin.[9]

In all families, whole exome sequencing was performed by exome capture [UM1: SeqCap EZ Exome v3.0 kit (Roche, CA, USA) at UM core facility; LUB1: NexteraRapid Exome Capture kit (Illumina, Inc., San Diego, CA, USA) at Centogene (Rostock, Germany); all NIJ cases: SureSelectXT Human All Exon 50Mb Kit V5 (Agilent, CA, USA) at BGI Copenhagen, and WF1 at GeneDx (Gaithersburg, MD, USA)] followed by next generation sequencing on Illumina arrays (UM1 and LUB1: paired end HiSeq2000; LUB1 NextSeq500), to medium coverage of 46X (UM1), and ~75X (all NIJ, LUB1, and WF1).

For UM1, two cases were sequenced and variant analysis was restricted to the ~10 Mb linkage

This article is protected by copyright. All rights reserved.

region. For LUB1, WF1 and NIJ4, parents were also sequenced and initially, a trio analysis for *de novo* variants (no damaging hits) was performed. Variants were called as follows: UM1.1 and UM1.4: Alignment was done using BWA against Human 1K Genome reference, duplicates were removed using Picard (v1.74), base recalibration, realignment and variant calling were done using GATK (v3.3); these samples were part of a 734-sample pooled call; LUB1: Variant calling was performed as described;[10] NIJ: Clinical exome sequencing and variant calling as described.[11] WF1: GeneDx clinical whole exome pipeline. Detected variants were filtered for rare (European population frequency <0.01) and protein-changing variants under a recessive model. VPS13D variants emerged as the strongest candidate in all cases.

All *VPS13D* variants were Sanger confirmed and segregation in the family consistent with compound heterozygosity was verified.

Copy number variant analysis was not performed on all samples. Since single exonic deletions are hard to detect in whole exome analyses, they hence can't be ruled out. Since all patients were compound heterozygous, a whole gene deletion in *VPS13D* can be ruled out.

Analysis of expression: Nonsense-mediated decay and splice site prediction

Since *VPS13D* expression is higher in skin (fibroblasts) than in blood, we used mRNA extracted from a fibroblast culture to study expression levels and nonsense-mediated mRNA decay in Family UM1 (data not shown) and Patient LUB1.1. For Patient LUB1.1, RNA was extracted using the QIAmp RNA Extraction Kit (QIAGEN, Germantown, MD, USA). Oligo-dT-Nucleotides of the Maxima First Strand cDNA Synthesis Kit (ThermoFisher, Waltham, MA, USA) served as primers to synthesize the complementary DNA (cDNA) by use of reverse transcriptase (RT). PCR was performed with primers in Exons 21 and 22 (VPS13Dex21F: TGATTCCTTAGTCCACATCAAC, VPS13Dex22R: ATCATTTCCAGGTGTGCTAC) and the respective product was inspected for its size and Sanger

This article is protected by copyright. All rights reserved.

Author Manuscript

sequenced. Further, the expression of VPS13D in LUB1.1 and a control was compared to the expression of *ß-Actin* and *HPRT*, and *YAZ* that served as reference genes. These quantitative PCRs were performed with SYBR Green on the LightCycler 480 system (data not shown). Since both qPCR and sequencing indicated instability of the allele with the nonsense mutation, we treated fibroblasts of LUB1.1 with cycloheximide for 8 hours at 100µg/ml final concentration to stabilize the transcript and confirm nonsense-mediated mRNA decay (NMD) as cause. Effect of cycloheximide was evaluated by sequencing of cDNA.

In addition to nonsense and missense mutations, we detected three variants at splice sites (c.941+3A>G, c.2237-1G>C, c.9998+4A>C). Since we are limited to perform skin biopsy for research purposes to adults only, per our IRB, we do not have fibroblast cultures from the children with splice mutations. Instead we used two online slice site prediction tools to estimate the impact of these variants on splicing: Human Splicing Finder (HSF, http://www.umd.be/HSF3/)[12] and Splice Site Prediction, set to mammals (SSP, http://www.fruitfly.org/seq_tools/splice.html). HSF provides a consensus value (CV) variation as output with the interpretation of CV <-10% indicating a disruption of the splice site. SSP generates a score between 0 and 1 with a score of 0.5 recognizing about 90% of the actual sites and a false-positive rate of <5%. The higher the score, the higher the probability that the splice site is active.

Comparison of mutation frequencies in *VPS13D* paralogs

To assess the impact of the loss of function of each *VPS13* paralogs, we compared phenotypes of animal models available in the literature and in databases, and examined estimates of mutation frequencies in humans. To assess the common mutation types (e.g. loss of function, missense) in each *VPS13* paralog-associated disease, we restricted analysis to cases in which both mutations are known.

Functional studies in patient-derived fibroblasts

From the UM1 family, we established fibroblast cell lines from two patients (UM1.2 and UM1.4) and two controls (UM1.17, a daughter of an affected, and UMCtrl1, a married-in unaffected spouse). From

This article is protected by copyright. All rights reserved.

Author Manuscript

LUB1, fibroblast lines were established from LUB1.1, the index patient, and her heterozygous parents (LUB1.3 and LUB1.4). In addition, fibroblasts from two unrelated control lines, LUBCtrl1, aka L-2132, and LUBCtrl2, aka L-2134, were used.

For mitochondrial imaging in fibroblast from the UM1 family, MitoTracker Red CMXRos (Invitrogen) was applied to fibroblasts cultured on coverslips for 40 minutes before fixing in 4% paraformaldehyde for 12 minutes. Through PLAPON 60X (1.42 Oil) lens on Olympus FV1000 confocal microscope, 6-8 z-stacks of images were obtained per visual field to produce images of in total 72 ~ 127 cells per line. Images were flattened using z-projection at maximum intensity using the open software Fiji,[13] which was also used to generate intensity histograms. For each 2-D image, the Otsu algorithm was applied to extract the top 1% brightest pixels. To quantify spherical mitochondria, any areas smaller than 1.5 μm^2 and with less circularity than 0.18 were removed using Fiji's Analyze Particles function. The remaining selected areas correspond to bright and spherical mitochondria. The average number of such selected objects per cell was calculated in each cell line. We also computed the percentage of cells with >2 such objects in the perinuclear region. Form factor analysis as a measurement of the mitochondrial network integrity was performed by using a selection algorithm in the software program Volocity (Perkin Elmer) to select mitochondrial objects (1 standard deviation above the mean MitoTracker intensity) of a projected Z-stack image (average intensity). For each projected image containing 4-12 cells, form factor defined as $[P_m^2]/[4\pi A_m]$ with P_m being the perimeter and A_m being the area of a mitochondrion, was calculated for all selected mitochondria and the mean was obtained for the entire image field. For each individual, 11-17 images from two independent experiments were analyzed.

In fibroblasts of Family LUB1, the form factor was determined as previously described.[14] In brief, the mitochondrial network in fibroblasts was stained with an anti-GRP75 antibody (1: 1000, Abcam, Cambridge, MA) in combination with the the Zenon immunolabelling kit (Invitrogen, Carlsbad, CA)

This article is protected by copyright. All rights reserved.

Author Manuscript

Author Manuscript

according to manufacturer's protocol. Based on single cell images, mitochondria area and outline were measured and the form factor was calculated. Mean form factor was averaged over 20 cells per individual.

Measurement of the rate of ATP synthesis in cultured fibroblasts

ATP was quantified, in triplicate, using the ATP Bioluminiscence Assay Kit CLS II (Roche Diagnostics), following manufacture's instruction. ATP is measured in a luminometer (Berthold, Detection System), and calculated as ATP generated (µMoles) per minute per mg of protein. The amount of protein was determined using the BCA protein Assay Kit (Pierce).

Functional studies in *Drosophila* models

All fly lines and related constructs were purchased from the Bloomington Stock Center, including Vps13D mutant lines [#56282 ($Vps13D^{11101}$) and 22996, only #56282 homozygous shown], Vps13D RNAi (#38320), motoneuron-specific Gal4 driver (D42-Gal4, #8816), a deficiency line Df(3L)Exel6117 (#7596), as well as fluorescent mitochondrial marker (UAS-mitoGFP, #42727).[15] All phenotypes observed of homozygous Vps13D mutant alleles were confirmed in compound heterozygous flies of the two alleles, and in mutant alleles over the deficiency line, which lacks a defined region of the *Drosophila* chromosome containing the entire Vps13D genetic locus and some neighboring genes. For staining, we used the following primary antibodies: ATP5A (Abcam ab14748), 1: 1000 GFP (Life Technologies A-11122, 1:1000), Horse Radish Peroxidase (HRP) (Jackson 123-605-021,1:1000), DLG (DSHB 4f3, 1:1000). All secondary antibodies were from Invitrogen (Alexa-conjugated 1:1000, 2 hrs, RT). Standard dissection and immunostaining procedures were used for larval tissue analysis.[16] For larval immunostaining, tissues were fixed with 4% formaldehyde for 20 minutes at room temperature prior to staining, except for anti-ATP5A staining in which tissue was fixed with Bouin's Fixative for 7 minutes at room temperature. Form factor analysis of larval ventral nerve cords was performed using Volocity to select mitochondrial networks in the cell bodies of RNAi expressing motoneurons based on threshold of

This article is protected by copyright. All rights reserved.

mitoGFP fluorescence (2.5 standard deviations above the mean fluorescence intensity) from a projected Z-stack image. For each cell body, an average form factor of all mitochondria was calculated.

Statistical analyses

Differences were analyzed statistically using unpaired t-tests, or analysis of variance (ANOVA) with a Bonferroni-Dunn post-hoc correction.

Author Manuscript

This article is protected by copyright. All rights reserved.

Author Manuscript

Results

Genetic Findings

Overview: In four different locations in the US and Europe, we independently detected compound heterozygous *VPS13D* mutations in 7 families. The mutational spectrum included five nonsense, five missense, one frameshift, one essential and two nonessential splice site mutations (Table 2). All families carried a combination of one loss-of-function mutation (LOF: nonsense, frameshift, or essential splice sites) and one presumably milder change (missense or nonessential splice site mutation).. All variants were absent or extremely rare (<13 heterozygous carriers) in the ~120,000 individuals listed in GnomAD. Among the five missense mutations, Gly1190Asp and Met1307Ile found in families UM1 and NIJ1 were located in the center of the protein. The three C-terminal missense mutations detected in families LUB1, NIJ2 and NIJ3 are close to or within the C-domain (Fig 1D), which is conserved and unique among all VPS13 proteins including yeast.

UM1 ataxia family (SCAR4): We have previously reported a family with 14 siblings, five of whom with adult-onset spinocerebellar ataxia with saccadic eye intrusion (Fig 1A, *SCAR4* [6, 7]). After exclusion of known ataxia mutations, genome-wide linkage analysis under a recessive, full penetrance model identified only a single locus with LOD > 0, which was 20 cM/ ~10 Mb on chromosome 1p36 flanked by rs7538691 and rs761162 (LOD = 3.1, data not shown). Whole exome sequencing in two affected individuals revealed compound heterozygous mutations in *VPS13D* as the only likely genetic cause within the linked region. The variants comprised a paternally inherited missense change (c.3569G>A, p.Gly1190Asp) and a maternally inherited stop-gain mutation (c.3316C>T, p.Gln1106Ter). Sanger sequencing verified segregation among all 12 siblings with available DNA samples. Sequencing of RT-PCR products from fibroblast cell lines of two patients demonstrated that the stop-gain allele-containing mRNA product was less abundant, suggesting that it underwent nonsense-mediated decay (data not shown). pGly1190Asp introduces an extra negative charge and appears not to affect protein stability

This article is protected by copyright. All rights reserved.

(data not shown).

Family LUB1: In two affected sisters of a German family with spastic ataxia (Fig 1B), we detected compound heterozygous mutations in *VPS13D* including a maternal nonsense mutation (Tyr1803Ter) and a paternal missense change (Ala4210Val, rs746736545). Similar to Family UM1, sequencing of cDNA of the index patient revealed the allele with the nonsense mutation to be less abundant. Treatment with cycloheximide stabilized the mutated allele and confirmed that the nonsense-mutated allele indeed underwent NMD (Fig 1C). NMD resulted in a decreased expression level of about 50-60% in Patient LUB1.1 (data not shown).

Additional sporadic cases: At the Radboudumc expert centre for genetic movement disorders in Nijmegen, and the genetic movement clinic in Rotterdam, the Netherlands, four unrelated cases of different ethnicities with compound heterozygous *VPS13D* mutations were independently identified (Table 1). NIJ1 and NIJ2 carry a combination of a nonsense mutation and a missense change, NIJ3 a frameshift and a non-essential splice site mutation, and NIJ4 carries an essential splice site mutation and a missense change (Table 2). NIJ4 also has optic atrophy and carries a heterozygous frameshift mutation in *OPA1* [c.1156_1157del (p.Leu386Glufs*2)]. A second (biallelic) mutation in *OPA1* was excluded by exome sequencing with sufficient coverage of the entire coding region and splice sites. Her mother carried the same variant and has isolated optic atrophy.

At the Wake Forest School of Medicine, Winston-Salem, North Carolina, USA, one additional case, WF1, was identified by clinical exome sequencing (GeneDx, Gaithersburg, MD). WF1 displayed hypotonia, balance and coordinating difficulties, as well as global developmental delay; more formal clinical ataxia tests were difficult to perform, due to her current age and disease features as well as global developmental delay. WF1 has a combination of a nonsense mutation and nonessential splice site change.

Author Manuscript

This article is protected by copyright. All rights reserved.

To estimate the impact of the splice site changes on the transcript, we used two different *in-silico* splice site prediction programs. As expected, both programs, HSF and SSP, strongly predicted an effect on splicing of the invariant acceptor splice site of intron 18 in NIJ4, c.2237-1G>C (Fig 2), which hence was classified LOF. The splice region variants in NIJ3 and WF1, however, are not within invariant splice consensus sites. For c.9998+4>C in intron 49, CV variation was -10.57%, thus just below HSF's -10 cut-off. SSP's prediction score dropped from 0.93 to 0.62 suggesting a mild, if any, impact on recognition of this splice site. For c.941+3A>G in intron 9, the CV variation was -0.83% by the HSF algorithm and would argue against an effect on splicing. However, the SSP score dropped from 0.89 to 0.21, suggesting reduction in predicted splicing ability. These two non-essential splice site mutations are hence not considered complete LOF alleles as they may allow some correctly spliced transcripts. Confirmatory analysis of intronic splice region variants could not be performed at this time (see methods for details).

Clinical findings

All cases except for WF1, which was too young, had either ataxia or spasticity as a core symptom. Onset ranged from infancy to early adulthood. The UM1 family, previously assigned *SCAR4*, demonstrated primarily adult-onset ataxia with distinct macrosaccadic intrusions[7], with pyramidal features, neuropathy, and myoclonus but no intellectual disability[6]. Videos of the clinical exams and the distinct eye phenotype are available in the online supplement of that reference[7]. The two sisters from family LUB1 were in their onset and clinical phenotypes similar to UM1, except for a different oculomotor phenotype. By contrast, NIJ1 had a much earlier onset (< 5 yrs) and symptoms were more debilitating (wheelchair-bound by age 17 yrs). Whether his phenotypic difference originates from more severe *VPS13D* mutations or other environmental or genetic factors is unknown at this time. Similarly, NIJ4 and WF1 were severely affected with an age at onset in the first year of life. In addition to ataxia and neuropathy, NIJ4 suffers from developmental delay, seizures, and optic atrophy. Coincidentally, she carries an additional mutation in *OPA1 (Optic Atrophy 1/ Mitochondrial Dynamin Like GTPase)*

This article is protected by copyright. All rights reserved.

Author Manuscript

which explains the optic atrophy but not the additional seizures and the developmental delay. NIJ2 was affected by spastic paraplegia without ataxia, with onset in early adulthood. Patients WF1 and NIJ3 might be more severely affected due to two severe mutations including a non-essential splice site change and a LOF mutation, in contrast to the combination of a missense and a LOF mutation in the other subjects.

Among *VPS13* paralogs, *VPS13D* is the most intolerant to mutations

Yeast *vps13* is implicated in many cellular functions including sporulation, Golgi organization, and mitochondrial integrity. [18] During metazoan evolution, two duplication events gave rise to three paralogs–*VPS13A/C, B, and D*. *Drosophila* Vps13 (CG2093) is an ortholog of *VPS13A/C,* which further duplicated in the vertebrate evolution into *VPS13A* and *VPS13C* (updated from reference [19]). Since not much is known about *VPS13D*-specific function, we compared reported phenotypes of VPS13 homologs in the two model organisms fly and mouse [fly database CG2093 [20], mouse: MGI2444304 [21], MGI2444207, and MGI2448530] (Table 3). Mutations in *Vps13D*/*VPS13D* cause embryonic lethality in both animals, while mutations in *VPS13A and C* appear more tolerable during early development (animal phenotypes for *VPS13B* are unavailable).

A similar trend was observed in human populations (Table 3): RVIS (Residual Variation Intolerance Score) is a gene-based intolerance score derived from allele frequency in whole exome sequence data.[22] Among the paralogs, *VPS13D* has the lowest RVIS score of -4.23, 0.14 percentile, suggesting *VPS13D* is among the most mutation-intolerant of human genes. We also compared the frequency of LOF in each paralog in the ExAC (Exome Aggregation Consortium) browser. Again, *VPS13D* emerges as most sensitive to LOF mutations, with the lowest ratio of the number of variants observed over expected. For *VPS13D*, the probability of LOF intolerance, pLI score, is 1, virtually certain. Indeed, chorea acanthocytosis is caused in 29/31 cases by LOF/LOF mutations in *VPS13A,*[23] Cohen syndrome in 41/45 cases by LOF/LOF mutations in *VPS13B,* [24-28] and Parkinson's disease in 3/4 cases by LOF/LOF mutations in *VPS13C* cases.[29, 30] In summary, *VPS13D* is intolerant to complete LOF of both

This article is protected by copyright. All rights reserved.

Author Manuscript

alleles, being likely incompatible with life, consistent with our finding of only compound heterozygous missense/LOF or nonessential splice/LOF mutations.

Vps13D disruption in *Drosophila* is lethal and causes mitochondrial defects

Known also as CG32113 in flies, fly Vps13D shows 33% protein identity to the human gene (Table 3). Consistent with *Vps13d* lethality in mice, flies disrupted for *Vps13D* do not survive beyond 2nd instar larvae stage. This lethality was confirmed with two independent lines containing large insertions in the coding region of *Vps13D*, including compound heterozygous animals containing one copy of each *Vps13D* allele, hence ruling out secondary mutations as the cause of lethality.

Since the only yeast vps13 protein has previously been implicated in mitochondrial function,[29] we hypothesized that loss of *Drosophila* Vps13D may alter mitochondria. In early 2nd instar larvae before lethality, we observed that deletion of *Vps13D* led to severe alterations in mitochondrial morphology. Instead of forming fine mitochondrial networks in individual cells, mitochondria appear as singular, enlarged objects. This abnormal mitochondrial appearance was present in the larval brain (Fig 2A) and other tissues in these young larvae (not shown). By contrast, no differences were detected for cellular markers of other organelles (Golgi, ER, lysosomes and the nucleus; data not shown).

We then used RNAi-mediated knockdown[31] to inhibit expression of *Vps13D* specifically in motoneurons. This allows for survival of larvae to the 3rd instar stage (death at pupal stage), which enables further characterization of Vps13D's autonomous function in neurons. By co-expression of mitoGFP targeted specifically to mitochondria of the RNAi depleted neurons,[15] we observed enlarged spherical mitochondria (Fig 2B). Compared to a control RNAi line targeting luciferase, knockdown by Vps13D RNAi resulted in a significant reduction in quantified form factor (Fig 2C), consistent with a loss of complexity of the mitochondria network coinciding with enlarged, isolated mitochondria. These observations suggest a role for Vps13D in regulating mitochondrial morphology and potentially also mitochondrial function in neurons.

The abnormal mitochondrial network in neuronal cell bodies led us to hypothesize that loss of Vps13D

This article is protected by copyright. All rights reserved.

Author Manuscript

would deleteriously impact the distribution of mitochondria to distal regions of neurons.

Previous studies have linked deficiencies in mitochondrial trafficking to distal neurites in neurodegenerative diseases and neuropathies.[32, 33] We observed that reduction of Vps13D in motoneurons led to strong impairment in the distribution of mitochondria in peripheral axons in segmental nerves (Fig 3A, B) and neuromuscular junction (NMJ) synapses (Fig 3C, D). The density of mitochondria was progressively reduced concomitant with increased distance from the cell body locations in the CNS (Fig 3). This failure to distribute mitochondria resembles previously described defects for mutations in mitochondrial fission/fusion machinery.[32]

Patient-derived fibroblasts show altered mitochondrial morphology

Given these fly data, we also investigated mitochondrial function and morphology in human fibroblasts. Staining fibroblasts from the affected subjects of family UM1 with MitoTracker, which accumulates in mitochondria in a membrane potential dependent manner, revealed significantly brighter mitochondria (Fig 4). While the typical mitochondrial network of elongated objects and branches was observed in both control and patient cells, the perinuclear regions of only affected cells often contained unusually bright and significantly more spherical mitochondrial objects, which were mostly in clusters and at higher magnification appeared to be donut-shaped (Fig 4G). To quantify the abundance of the bright and spherical mitochondria in each cell line, we extracted the top 1% brightest pixels from each image and selected circular objects based on computed circularity score. The average number of such abnormal mitochondrial objects was ~ 6-fold higher in the affected compared to control cells (Fig 4H). In the perinuclear region, such objects were identified in clusters (≥ 3) in ~10% of normal but 91% and 67% of fibroblasts of affected subjects' cells (Fig 4I). Consistent with the *Drosophila* data, form factor analysis also revealed a significant reduction in the degree of mitochondrial branching in the affected fibroblasts compared to controls (Fig 4J). These observations suggest structural defects in mitochondria in VPS13D-deficient fibroblasts.

This article is protected by copyright. All rights reserved.

Author Manuscript

Author Manuscript

Independent analysis of fibroblasts of the proband of family LUB1 demonstrated that the affected fibroblasts expressed reduced levels of mitochondrial GRP75 protein compared to controls (Fig 5A-C). Form factor analysis of GRP75 immunostaining revealed a similar reduction in the degree of mitochondrial branching of proband fibroblasts compared to two unrelated healthy controls (Fig 5D). These structural mitochondrial changes were accompanied by a reduced ATP production rate of LUB1.1 compared to control fibroblasts (Fig 5E).

Discussion

In this study, we have identified seven different compound heterozygous mutations in *VPS13D* in twelve patients and link VPS13D/Vps13D defects in patient fibroblasts and in flies to mitochondrial deficits. Our study also included a large family with ataxia (*SCAR4*) and linkage to a 10-Mb region on chromosome 1p36 including the *VPS13D* gene.

The core phenotype of the eleven patients above the age of 2 with compound heterozygous *VPS13D* mutations is characterized by movement disorders of the ataxia-spasticity spectrum, ranging from predominant ataxia, spastic ataxia, to spastic paraplegia without ataxia, and ataxia plus phenotypes. The latter included two cases with an additional developmental delay phenotype (NIJ3 and NIJ4). The youngest patient, WF1 of age 2 at the last evaluation, presented with hypotonia, developmental delay, including motor delay, and was not yet ambulatory. These three patients also have different types or additional mutations, as NIJ3 and WF1 carry nonessential splice region variants in addition to an LOF. This may be more severe than the combination of missense/LOF found in the other cases. In addition, NIJ4's presentation may be complicated by an additional mutation in *OPA1*. The protein encoded by *OPA1* is also implicated in mitochondrial function. It is conceivable that there may be an interactive effect of the two mutations linked to mitochondrial dysfunction. Interestingly, recent data have shown that about 5% of patients carry two independent Mendelian diseases. [34] However, digenic inheritance can't be ascertained based on this single case. Of note, homozygous or compound heterozygous *OPA1*

This article is protected by copyright. All rights reserved.

mutations cause an extended multi-system phenotype that includes ataxia and spastic paraplegia, known as Behr syndrome. [17] While there was complete coverage of the *OPA1* coding regions and splice sites, no second mutation in the *OPA1* gene was detected by exome nor by copy number analyses (conducted as described)[35]. Hence, although we cannot exclude an undetected intronic or promoter mutation that is not penetrant, as the father does not have optic atrophy, we believe Behr syndrome as an alternative diagnosis in this case is not likely.

The overlap between genetic forms of ataxias and hereditary spastic paraplegias is well recognized, as there are other examples of genes (e.g., *SPG7*) that when mutated can give rise to either pure ataxia or spastic paraplegia or to a mixed phenotype of spastic ataxia,[36, 37] developmental delay, and seizures, and other complex phenotypes commonly accompany early onset recessive ataxias.[2] In addition, there was variability in age of onset in our patients, which is also not unusual for ataxias. Frequently observed neurological co-morbidities in our series included peripheral axonal neuropathy and extrapyramidal signs such as myoclonus and dystonia. Infertility was noted in two male cases. Although it is currently uncertain whether this is *VPS13D*-related, infertility is a known feature of mitochondrial disease.[38]

VPS13D encodes a large protein (4388 amino acids), whose paralogs cause other neurological disorders: *VPS13A* mutations cause chorea acanthocytosis, characterized by a severe hyperkinetic movement disorder, myopathy, epileptic seizures, cognitive decline and behavioral changes, [23, 39] and perturb protein homeostasis in the fly.[20] *VPS13B* is involved in Cohen syndrome [40, 41] and *VPS13C* in rare cases of genetic Parkinson's disease with mitochondrial dysregulation and mitophagy. [29] Most of these disease-associated mutations are LOF/LOF (see Table 3). In contrast to the other VPS13 paralogs, knocking out *VPS13D's* homologs in *Drosophila* (our results) and mouse (MGI:2448530) leads to embryonic lethality, and not a single LOF/LOF mutation was identified, suggesting that some residual VPS13D function in humans may be critical for survival. In addition, the ExAC server's pLI

This article is protected by copyright. All rights reserved.

score, i.e. the probability that a gene may be intolerant to haploinsufficiency, for *VPS13D* is 1, in contrast to all other *VPS13* genes (Table 3). [42] We did not, however, observe the predicted intolerance to haploinsufficiency, as one parent of each of the cases reported here was haploinsufficient, but none were symptomatic, including one parent who lived into their 90s without apparent neurological problems.

Our genetic data allow for some first, yet cautious speculations on genotype-phenotype correlations. First, our current data collectively point to missense/LOF mutations tending to cause relatively pure ataxia and/or spasticity. Second, as suggested by the more severe NIJ3 and WF1 cases, who carry non-essential splice site/LOF mutations, other mutation type combinations may be associated with a broader and/or more severe spectrum of phenotypes. Lastly, the other severe case, NIJ4, had a co-existent dominant *OPA1* mutation and corresponding optic atrophy,[43] which was also observed in the subject's mother. The *OPA1* mutation may contribute epistatically to the phenotype since *OPA1* also affects mitochondrial function.[43]

Although our study convincingly establishes missense/LOF mutations in *VPS13D* as causing ataxia/spastic paraplegia and mitochondrial pathology, many questions remain to be addressed. Clinically, predicting the phenotype from new mutations in *VPS13D* will be difficult. Even for missense/LOF mutation carriers, the clinical presentation varied in our series. In addition, homozygous or compound heterozygous missense mutations were not observed here. As *VPS13D* is a large gene with many missense variants reported in databases including homozygosity,[42] it will be even more difficult to predict pathogenicity of any novel biallelic missense variants.

While further work is warranted to pin down the precise mitochondrial defect, we have shown abnormal mitochondrial morphology in both flies and patient cell lines, and reduced mitochondrial function in fibroblasts. Mitochondrial dysfunction is associated with several other ataxias and spastic

This article is protected by copyright. All rights reserved.

paraplegias such as Friedreich's ataxia,[44] *SCA28*,[45] *POLG*,[46] and *SPG7*,[47] as well as in some unexplained ataxias.[48] Although we observed a defect in mitochondrial distribution in both *Drosophila* neurons lacking Vps13D and patient fibroblasts containing mutations in *VPS13D*, the precise biological underpinnings of this defect are still under investigation, including electron microscopy studies to assess mitochondrial morphology. Alterations of mitochondrial dynamics such as transport, fission, and/or fusion[32] can all potentially manifest in aberrant distribution of mitochondria throughout the cell. Various mutations in mitochondrial genes lead to the production of reactive oxygen species,[49] which can additionally disrupt mitochondrial distribution in neurons. Combining the *in vitro* cellular model of patient fibroblasts and neurons differentiated from induces pluripotent stem cells with *in vivo* experiments in the genetic fly model may help us parse out the cellular role of VPS13D in mitochondrial biology and disease progression. These methods will also allow for testing of potential therapies that target mitochondrial dysfunction and that could be common to other forms of ataxia and spastic paraplegias.

While this manuscript was under review, Anding et al. published findings showing VPS13D to be a ubiquitin-binding protein and affecting mitochondrial fission and fusion, [50] consistent with our findings, and also implemented VPS13D in autophagy, a process that we have recently reported to be involved in ataxia. [51]

Author

Acknowledgment

We thank the patients for their willingness to participate and patience during our research. We thank Dr. Philipp Capetian for clinical evaluation of Family LUB1 and referring to the study. Linda Gates, Thomas Kubisiak, and Frauke Hinrichs for excellent technical assistance; Johann Gudjonsson, MD (Dermatology, University of Michigan) for fibroblast biopsies, Soochin Cho (Creighton University) for useful discussion on VPS13 evolution; Bart Post, MD, PhD and Jolanda Schieving, MD (Department of Neurology, Radboud university medical centre, Nijmegen, the Netherlands) and M. Jongen, MD, PhD

This article is protected by copyright. All rights reserved.

(Department of Neurology, Erasmus MC, Rotterdam, the Netherlands) and Aasef Shaikh, MD (Neurology, Case Western Reserve) for providing important clinical data.

This work was supported by the US National Institutes of Health grants NS056780 (MB), NS069844 (CC), and F32NS098611 (RI), the National Ataxia Foundation (MB), European Union's Horizon 2020 research innovation program under the ERA-NET Cofund action N° 643578, ZonMW (9003037604; BvdW) under the frame of the E-Rare-3 network PREPARE, the Hersenstichting (BvdW), Radboud university medical centre (BvdW) and Bioblast Pharma (BvdW), the Foundation of the University Hospital Schleswig-Holstein ("Gutes Tun!", AM), and a career development award from the Hermann and Lilly Schilling Foundation (CK).

Author Contributions:

JZL, AM, VS, CK, CC, KL, BvdW, MB contributed to the conception and design of the study

ESe, RI, MD, E-JK, JT, NB, ESa, SL, ABO, TJ, AJAK contributed to acquisition and analysis of data

ESe, RI, MD, E-JK, CK, CC, KL, BvdW, MB contributed to drafting the text and preparing the figures

Potential Conflicts of Interests:

None of the authors report COI relevant to the reported work. See disclosures for other detailed COI

Author Manuscript

This article is protected by copyright. All rights reserved.

Author Manuscript

Literature Cited

1. Sandford E, Burmeister M. Genes and genetic testing in hereditary ataxias. Genes (Basel). 2014;5(3):586-603.

2. Beaudin M, Klein CJ, Rouleau GA, Dupre N. Systematic review of autosomal recessive ataxias and proposal for a classification. Cerebellum Ataxias. 2017;4:3.

3. Marras C, Lang A, van de Warrenburg BP, et al. Nomenclature of genetic movement disorders: Recommendations of the International Parkinson and Movement Disorder Society task force. Mov Disord. 2017 May;32(5):724-5.

4. Fogel BL, Lee H, Deignan JL, et al. Exome sequencing in the clinical diagnosis of sporadic or familial cerebellar ataxia. JAMA Neurol. 2014 Oct;71(10):1237-46.

5. Synofzik M, Schule R. Overcoming the divide between ataxias and spastic paraplegias: Shared phenotypes, genes, and pathways. Mov Disord. 2017 Mar;32(3):332-45.

6. Swartz BE, Burmeister M, Somers JT, Rottach KG, Bespalova IN, Leigh RJ. A form of inherited cerebellar ataxia with saccadic intrusions, increased saccadic speed, sensory neuropathy, and myoclonus. Ann N Y Acad Sci. 2002 Apr;956:441-4.

7. Swartz BE, Li S, Bespalova I, et al. Pathogenesis of clinical signs in recessive ataxia with saccadic intrusions. Ann Neurol. 2003 Dec;54(6):824-8.

8. Sobreira N, Schiettecatte F, Valle D, Hamosh A. GeneMatcher: a matching tool for connecting investigators with an interest in the same gene. Hum Mutat. 2015 Oct;36(10):928-30.

9. Abecasis GR, Cherny SS, Cookson WO, Cardon LR. Merlin--rapid analysis of dense genetic maps using sparse gene flow trees. Nat Genet. 2002 Jan;30(1):97-101.

10. Trujillano D, Bertoli-Avella AM, Kumar Kandaswamy K, et al. Clinical exome sequencing: results from 2819 samples reflecting 1000 families. Eur J Hum Genet. 2017 Feb;25(2):176-82.

11. van de Warrenburg BP, Schouten MI, de Bot ST, et al. Clinical exome sequencing for cerebellar ataxia and spastic paraplegia uncovers novel gene-disease associations and unanticipated rare disorders. Eur J Hum Genet. 2016 Oct;24(10):1460-6.

This article is protected by copyright. All rights reserved.

12. Desmet FO, Hamroun D, Lalande M, Collod-Beroud G, Claustres M, Beroud C. Human Splicing Finder: an online bioinformatics tool to predict splicing signals. Nucleic Acids Res. 2009 May;37(9):e67.

13. Schindelin J, Arganda-Carreras I, Frise E, et al. Fiji: an open-source platform for biological-image analysis. Nat Methods. 2012 Jun 28;9(7):676-82.

14. Grunewald A, Voges L, Rakovic A, et al. Mutant Parkin impairs mitochondrial function and morphology in human fibroblasts. PLoS One. 2010 Sep 27;5(9):e12962.

15. Pilling AD, Horiuchi D, Lively CM, Saxton WM. Kinesin-1 and Dynein are the primary motors for fast transport of mitochondria in Drosophila motor axons. Mol Biol Cell. 2006 Apr;17(4):2057-68.

16. Klinedinst S, Wang X, Xiong X, Haenfler JM, Collins CA. Independent pathways downstream of the Wnd/DLK MAPKKK regulate synaptic structure, axonal transport, and injury signaling. J Neurosci. 2013 Jul 31;33(31):12764-78.

17. Carelli V, Sabatelli M, Carrozzo R, et al. 'Behr syndrome' with OPA1 compound heterozygote mutations. Brain. 2015 Jan;138(Pt 1):e321.

18. Myers MD, Payne GS. Vps13 and Cdc31/centrin: Puzzling partners in membrane traffic. J Cell Biol. 2017 Feb;216(2):299-301.

19. Velayos-Baeza A, Vettori A, Copley RR, Dobson-Stone C, Monaco AP. Analysis of the human VPS13 gene family. Genomics. 2004 Sep;84(3):536-49.

20. Vonk JJ, Yeshaw WM, Pinto F, et al. Drosophila Vps13 Is Required for Protein Homeostasis in the Brain. PLoS One. 2017;12(1):e0170106.

21. Tomemori Y, Ichiba M, Kusumoto A, et al. A gene-targeted mouse model for chorea-acanthocytosis. J Neurochem. 2005 Feb;92(4):759-66.

22. Petrovski S, Gussow AB, Wang Q, et al. The Intolerance of Regulatory Sequence to Genetic Variation Predicts Gene Dosage Sensitivity. PLoS Genet. 2015 Sep;11(9):e1005492.

23. Dobson-Stone C, Velayos-Baeza A, Jansen A, et al. Identification of a VPS13A founder mutation in French Canadian families with chorea-acanthocytosis. Neurogenetics. 2005 Sep;6(3):151-8.

This article is protected by copyright. All rights reserved.

Author Manuscript

24. Hennies HC, Rauch A, Seifert W, et al. Allelic heterogeneity in the COH1 gene explains clinical variability in Cohen syndrome. Am J Hum Genet. 2004 Jul;75(1):138-45.

25. Katzaki E, Pescucci C, Uliana V, et al. Clinical and molecular characterization of Italian patients affected by Cohen syndrome. J Hum Genet. 2007;52(12):1011-7.

26. Kolehmainen J, Wilkinson R, Lehesjoki AE, et al. Delineation of Cohen syndrome following a large-scale genotype-phenotype screen. Am J Hum Genet. 2004 Jul;75(1):122-7.

27. Seifert W, Holder-Espinasse M, Kuhnisch J, et al. Expanded mutational spectrum in Cohen syndrome, tissue expression, and transcript variants of COH1. Hum Mutat. 2009 Feb;30(2):E404-20.

28. Seifert W, Holder-Espinasse M, Spranger S, et al. Mutational spectrum of COH1 and clinical heterogeneity in Cohen syndrome. J Med Genet. 2006 May;43(5):e22.

29. Lesage S, Drouet V, Majounie E, et al. Loss of VPS13C Function in Autosomal-Recessive Parkinsonism Causes Mitochondrial Dysfunction and Increases PINK1/Parkin-Dependent Mitophagy. Am J Hum Genet. 2016 Mar 3;98(3):500-13.

30. Schormair B, Kemlink D, Mollenhauer B, et al. Diagnostic exome sequencing in early-onset Parkinson's disease confirms VPS13C as a rare cause of autosomal-recessive Parkinson's disease. Clin Genet. 2017 Sep 01.

31. Dietzl G, Chen D, Schnorrer F, et al. A genome-wide transgenic RNAi library for conditional gene inactivation in Drosophila. Nature. 2007 Jul 12;448(7150):151-6.

32. Baloh RH. Mitochondrial dynamics and peripheral neuropathy. Neuroscientist. 2008 Feb;14(1):12-8.

33. Yu Y, Lee HC, Chen KC, et al. Inner membrane fusion mediates spatial distribution of axonal mitochondria. Sci Rep. 2016 Jan 08;6:18981.

34. Posey JE, Harel T, Liu P, et al. Resolution of Disease Phenotypes Resulting from Multilocus Genomic Variation. N Engl J Med. 2017 Jan 5;376(1):21-31.

35. Pfundt R, Del Rosario M, Vissers L, et al. Detection of clinically relevant copy-number variants by exome sequencing in a large cohort of genetic disorders. Genet Med. 2017 Jun;19(6):667-75.

This article is protected by copyright. All rights reserved.

Author Manuscript

36. de Bot ST, Willemsen MA, Vermeer S, Kremer HP, van de Warrenburg BP. Reviewing the genetic causes of spastic-ataxias. Neurology. 2012 Oct 02;79(14):1507-14.

37. van Gassen KL, van der Heijden CD, de Bot ST, et al. Genotype-phenotype correlations in spastic paraplegia type 7: a study in a large Dutch cohort. Brain. 2012 Oct;135(Pt 10):2994-3004.

38. Demain LA, Conway GS, Newman WG. Genetics of mitochondrial dysfunction and infertility. Clin Genet. 2017 Feb;91(2):199-207.

39. Tomiyasu A, Nakamura M, Ichiba M, et al. Novel pathogenic mutations and copy number variations in the VPS13A gene in patients with chorea-acanthocytosis. Am J Med Genet B Neuropsychiatr Genet. 2011 Jul;156B(5):620-31.

40. Balikova I, Lehesjoki AE, de Ravel TJ, et al. Deletions in the VPS13B (COH1) gene as a cause of Cohen syndrome. Hum Mutat. 2009 Sep;30(9):E845-54.

41. Megarbane A, Slim R, Nurnberg G, Ebermann I, Nurnberg P, Bolz HJ. A novel VPS13B mutation in two brothers with Cohen syndrome, cutis verticis gyrata and sensorineural deafness. Eur J Hum Genet. 2009 Aug;17(8):1076-9.

42. Exome Aggregation Consortium (ExAC). Cambridge, MA2015 [updated 2015/01/16/]; Available from: http://exac.broadinstitute.org.

43. Chun BY, Rizzo JF, 3rd. Dominant optic atrophy: updates on the pathophysiology and clinical manifestations of the optic atrophy 1 mutation. Curr Opin Ophthalmol. 2016 Nov;27(6):475-80.

44. Jasoliya MJ, McMackin MZ, Henderson CK, Perlman SL, Cortopassi GA. Frataxin Deficiency Impairs Mitochondrial Biogenesis in Cells, Mice and Humans. Hum Mol Genet. 2017 Apr 21.

45. Pierson TM, Adams D, Bonn F, et al. Whole-exome sequencing identifies homozygous AFG3L2 mutations in a spastic ataxia-neuropathy syndrome linked to mitochondrial m-AAA proteases. PLoS Genet. 2011 Oct;7(10):e1002325.

46. Finsterer J. Ataxias with autosomal, X-chromosomal or maternal inheritance. Can J Neurol Sci. 2009 Jul;36(4):409-28.

Author Manuscript

This article is protected by copyright. All rights reserved.

47. Shanmughapriya S, Rajan S, Hoffman NE, et al. SPG7 Is an Essential and Conserved Component of the Mitochondrial Permeability Transition Pore. Mol Cell. 2015 Oct 01;60(1):47-62.

48. Bargiela D, Shanmugarajah P, Lo C, et al. Mitochondrial pathology in progressive cerebellar ataxia. Cerebellum Ataxias. 2015;2:16.

49. Hayashi G, Cortopassi G. Oxidative stress in inherited mitochondrial diseases. Free Radic Biol Med. 2015 Nov;88(Pt A):10-7.

50. Anding AL, Wang C, Chang TK, et al. Vps13D Encodes a Ubiquitin-Binding Protein that Is Required for the Regulation of Mitochondrial Size and Clearance. Curr Biol. 2017 Dec 30.

51. Kim M, Sandford E, Gatica D, et al. Mutation in ATG5 reduces autophagy and leads to ataxia with developmental delay. Elife. 2016 Jan 26;5.

Author Manuscript

This article is protected by copyright. All rights reserved.

Author Manuscript

Figure Legends:

Figure 1. Multiplex ataxia families with compound heterozygous mutations in *VPS13D*

A. Pedigree of Family UM1. Affected siblings are indicated by black filled symbols while unaffected individuals are marked by unfilled symbols. The nine unaffected siblings are shown in an open diamond. Mutational status is given below each individual together with the respective laboratory ID. **B.** Pedigree of Family LUB1 with mutations in the two affected sisters, shown by black filled symbols. **C.** cDNA sequences of the c.5409C>A mutation before (top panel) and after (lower panel) treatment with cycloheximide. The traces are representative of 2 sequencing runs. The nonsense-mutated allele got stabilized and showed similar expression levels upon treatment. **D.** Predicted domain maps of VPS13D protein (http://www.ebi.ac.uk/interpro/protein/Q5THJ4) with the identified missense mutations marked: N1: VPS13 1st N-terminal domain (aa 2-115), N2: VPS13 2nd N-terminal domain (aa 137-356), U: UBA (Ubiquitin-associated)-like domain (aa 2627-2679), SHR: VPS13 SHORT ROOT transcription factor-binding domain (aa 3276-3558), C: VPS13 C-terminal domain (aa 3983-4129). The five different missense mutations appear to cluster in two regions, one in the middle and the other near the C domain. **E**. Amino acid sequence alignments of the regions surrounding each missense mutation across various species. While Gly1190Asp, Asn4107Ile, and Gly4149Ser are conserved in all VPS13D orthologs, Met1307Leu and Ala4210Val are conserved in mammals and chicken but not in zebrafish and/or fruitfly.

This article is protected by copyright. All rights reserved.

Figure 2. Disruption of *Vps13D* in the *Drosophila* central nervous system affects mitochondrial morphology.
A. Ventral nerve cord (VNC), stained for mitochondrial marker ATP5A, of control (w^{1118}, right panel) and *Vps13D* mutant (*Vps13D*$^{11101/11101}$, left panel) *Drosophila* larvae. Bottom: High magnification single confocal Z-planes of areas indicated by the dashed boxes, highlighting mitochondrial morphology in neuronal cell bodies. Scale Bars: 50µm (top) and 5µm (bottom) **B**. Representative images of motoneurons (via D42-Gal4) with simultaneous expression of fluorescent mitochondrial marker mitoGFP (green) along with control (left panel) and *Vps13D* (right panel) RNAi expression. Bottom: High magnification single confocal Z-planes of areas indicated by the dashed boxes, highlighting mitochondrial morphology in motoneuron cell bodies. **C.** Quantification of form factor analysis of the mitochondrial network (based on mitoGFP) in neuronal cells bodies expressing control RNAi (white) vs. *Vps13D* RNAi (grey). n=50 neurons per condition (from 5 different animals). Error bars represent standard error. *** indicates p<0.001 (Students T-test).

Author Manuscript

This article is protected by copyright. All rights reserved.

Figure 3: Knockdown of *Vps13D* in *Drosophila* motoneurons disrupts the distribution of mitochondria to distal axons.

A. Segmental nerves (HRP, red) containing motoneuron axons expressing fluorescent mitochondrial marker mitoGFP (green) of control RNAi and Vps13D RNAi knockdown (RNAi) animals. Nerves near the VNC (proximal, top) and distant from the VNC (distal, bottom) are shown. Scale Bar: 10μm. **B**. Quantification of the mitochondrial content per area within segmental nerves in proximal and distal regions of motoneurons expressing control RNAi (white) vs. *Vps13D* RNAi (grey). Data is normalized to Control RNAi Proximal Region condition. n≥10 individual nerves from 5 different animals. Error bars represent standard error. **** indicates p<0.0001 (Students T-test). **C**. Larval NMJ synapses from motoneuron axons expressing fluorescent mitochondrial marker mitoGFP (green) of control and Vps13D RNAi knockdown animals. HRP (red) labels neuronal membrane, while DLG (blue) labels NMJ postsynaptic region. High magnification images of the synaptic region (indicated by the dashed box) are shown (right panels) to highlight mitochondria occupying the synaptic region. Scale Bar: 20μm (left) and 2.5μm (right). **D**. Quantification of the mitochondrial content in the NMJ synapse per area of motoneurons expressing control RNAi (white) vs. *Vps13D* RNAi (grey). Data is normalized to Control RNAi condition. n=5 animals (each n represents the avg. mitochondrial content of ≥6 NMJ synapses/animal). Error bars represent standard error. **** indicates p<0.0001 (Students T-test).

Author Manuscript

This article is protected by copyright. All rights reserved.

Figure 4. Patient fibroblasts contain abnormal spherical mitochondria

A-D: Comparison of mitochondria in 4 fibroblast lines of Family UM1 stained with MitoTracker: A, UMCtrl1: wild type for *VPS13D*; B, UM1.17: asymptomatic heterozygous carrier of the Gly1190Asp missense mutation; C and D, UM1.2 and UM1.4: VPS13D compound heterozygous patients. Note that while the majority of the mitochondria in the control cells are elongated and of similar intensity, the patient cells are loaded with particularly bright, circular mitochondrial objects mostly localized in perinuclear region. **E**: Intensity histogram of MitoTracker images. The X-axis represents the intensity, the numbers of pixels are plotted on the Y-axis (the black plots in natural number scale and the gray plot in log-scale). Note that both patients have many more pixels with higher intensity, indicative of the increase in bright MitoTracker-stained objects. **F** and **G**: Perinuclear mitochondria at higher magnification (60X lens, 4X zoom). Control mitochondria (F, UMCtrl1) are elongated, tubular, and interconnected while the patient mitochondria (G, UM1.2) are often donut-shaped. Here, brightness was individually optimized to reveal the structural details and is not comparable. Scale Bars: 20 μm (A-D) and 2 μm (F and G). **H**: Average number of circular mitochondria (MT) objects identified by image processing. Such circular objects are present in the control cell lines at low frequencies but become much more abundant in the affected cell lines (~6-fold increase). **I**: Percentage of cells with at least 3 perinuclear circular MT objects. The patient fibroblast cultures have higher number of cells with perinuclear circular MT objects than control (6- and 9-fold increase). **J.** Form factor analysis of the mitochondrial network stained by MitoTracker. In H to J, error bars represent standard error. *, **, and *** indicate $p<10^{-4}$, $p<10^{-5}$, and $p<10^{-6}$ respectively (Student's T-test).

Author Manuscript

This article is protected by copyright. All rights reserved.

Figure 5. Altered mitochondrial morphology and decreased ATP in *VPS13D* mutant fibroblasts. **A.** Western blot analysis shows mitochondrial GRP75 protein levels in the *VPS13D*-mutant fibroblasts (LUB1.1), patient's parents (LUB1.3 and LUB1.4), and healthy control fibroblasts (LUBCtrl2) with β-actin as loading control. **B.** Quantification of the above GRP75 Western blot using ImageJ. **C.** The mitochondrial network was investigated under basal conditions by confocal microscopy in fixed cells immunostained with anti-GRP75. Scale Bar: 20 μm. **D.** Form factor as a measure for mitochondrial interconnectivity (GRP75 immunostaining) was calculated for two control fibroblast lines (LUBCtrl1, LUBCrtl2) and one patient line (LUB1.1) (n=20). Each dot represents measurement in a single cell. The mean values, and the standard deviations of the investigated individuals are shown. **E.** ATP production was determined based on luminescence. ATP concentration (μmoles) was calculated per minute per milligram of protein (n=3 independent experiments). In B and E, the error bars indicate SEM of n≥3 independent experiments.

Author Manuscript

This article is protected by copyright. All rights reserved.

Author Manuscript

Mutations in *VPS13D* lead to a new recessive ataxia with spasticity and mitochondrial defects

RUNNING TITLE: VPS13D in ataxia/spastic paraplegia

Eunju Seong[1], PhD, Ryan Insolera[2], PhD, Marija Dulovic[3], PhD, Erik-Jan Kamsteeg[4], PhD, Joanne Trinh[3], PhD, Norbert Brüggemann[5], MD, Erin Sandford[1], PhD, Sheng Li[13], PhD, Ayse Bilge Ozel[6], PhD, Jun Z. Li[6,7], PhD, Tamison Jewett[8], MD, Anneke J.A. Kievit[9], MD PhD, Alexander Münchau[3], MD, Vikram Shakkottai[10], MD PhD, Christine Klein[3], MD, Catherine Collins[2], PhD, Katja Lohmann[3*], PhD, Bart P. van de Warrenburg[11*], MD PhD, Margit Burmeister[1,6,7,12*], PhD

Affiliations

[1]Molecular & Behavioral Neuroscience Institute, University of Michigan, Ann Arbor, MI 48109, USA.

[2]Department of Molecular, Cellular, and Developmental Biology, University of Michigan, Ann Arbor, MI 48109, USA.

[3]Institute of Neurogenetics, University of Lübeck, Germany

[4]Department of Human Genetics, Radboud University Medical Centre, Nijmegen, The Netherlands

[5]Department of Neurology, University of Lübeck, Germany

[6]Department of Human Genetics, University of Michigan, Ann Arbor, MI 48109, USA.

[7]Department of Computational Medicine & Bioinformatics, University of Michigan, Ann Arbor, MI 48109, USA.

[8]Department of Pediatrics, Section on Medical Genetics, Wake Forest School of Medicine, Winston-Salem, North Carolina, USA.

[9]Department of Clinical Genetics, Erasmus MC, Rotterdam, the Netherlands

[10]Departments of Neurology and of Molecular and Integrative Physiology, University of Michigan, Ann Arbor, MI 48109, USA

This article is protected by copyright. All rights reserved.

Author Manuscript

[11]Department of Neurology, Donders Institute for Brain, Cognition and Behaviour, Radboud University Medical Center, Nijmegen, The Netherlands

[12]Department of Psychiatry, University of Michigan, Ann Arbor, MI 48109, USA.

[13]Present Address: Bio-X Center, Shanghai Jiao Tong University, China.

*Corresponding authors:

Margit Burmeister
Molecular & Behavioral Neuroscience Institute
University of Michigan
5061 BSRB, 109 Zina Pitcher Place
Ann Arbor MI 48109-2200
+1 734 647 2186
margit@umich.edu

Bart van de Warrenburg
Department of Neurology 935
Donders Institute for Brain, Cognition and Behaviour,
Radboud University Medical Center
P.O. Box 9101,
6500 HB, Nijmegen, The Netherlands
+31-24-3613396
Bart.vandeWarrenburg@radboudumc.nl

Katja Lohmann
Institute for Neurogenetics
University of Lübeck
Maria-Goeppert-Straße 1
23562 Lübeck, Germany
+49 451 3101 8209
katja.lohmann@neuro.uni-luebeck.de

This article is protected by copyright. All rights reserved.

Author Manuscript

Abstract:

Objective: To identify novel causes of recessive ataxias, including spinocerebellar ataxia with saccadic intrusions, spastic ataxias and spastic paraplegia.

Methods: In an international collaboration, we independently performed exome sequencing in seven families with recessive ataxia and/or spastic paraplegia. To evaluate the role of *VPS13D* mutations, we evaluated a *Drosophila* knock-out model and investigated mitochondrial function in patient-derived fibroblast cultures.

Results: Exome sequencing identified compound heterozygous mutations in *VPS13D* on chromosome 1p36 in all seven families. This included a large family with 5 affected siblings with spinocerebellar ataxia with saccadic intrusions (*SCASI*), or spinocerebellar ataxia, recessive, type 4, *SCAR4.* Linkage to chromosome 1p36 was found in this family with a LOD score of 3.1. The phenotypic spectrum in our 12 patients was broad. Although most presented with ataxia, additional or predominant spasticity was present in 5 patients. Disease onset ranged from infancy to 39 years, and symptoms were slowly progressive and included loss of independent ambulation in 5. All but two patients carried a loss-of-function (nonsense or splice site) mutation on one and a missense mutation on the other allele. Knock-down or removal of *Vps13D* in *Drosophila* neurons led to changes in mitochondrial morphology and impairment in mitochondrial distribution along axons. Patient fibroblasts showed altered morphology and functionality including reduced energy production.

Interpretation: Our study demonstrates that compound heterozygous mutations in *VPS13D* cause movement disorders along the ataxia-spasticity spectrum, making *VPS13D* the fourth VPS13 paralog involved in neurological disorders.

This article is protected by copyright. All rights reserved.

Author Manuscript

Introduction

Ataxia is a symptom of over 400 syndromic neurological conditions or can be the sole symptom of >80 recessively, dominantly, or X-linked inherited genetically defined conditions.[1-3] Recessive forms of ataxia are clinically and genetically more heterogeneous than dominant ataxias., ~~and~~ O~~o~~nly in a minor fraction (~20%) of idiopathic or suspected recessive ataxia cases can a mutation in a known ataxia gene be identified,[4] suggesting that much of the genetic heterogeneity still remains to be discovered. In addition to heterogeneity, there is also pleiotropy, as the spectrum of ataxias also includes clinical and molecular overlap with, for example, the spastic paraplegias.[5]

Here, we report 12 patients from 7 families with compound heterozygous mutations in *VPS13D*. All patients > 2 years old have ataxia and/or spasticity, while the one 2 year old patient shows developmental delay, hypotonia, and is nonambulatory (Table 1). The phenotype in one of these families, comprising 5 patients (Figure 1), has previously been described in detail.[6, 7] Briefly, patients in this family demonstrated early adult-onset cerebellar ataxia with neuropathy and pyramidal signs, as well as striking saccadic intrusions, hence initially referred to as spinocerebellar ataxia with saccadic intrusion (*SCASI*)., [6] later renamed spinocerebellar ataxia, recessive 4 (*SCAR4)*. Analysis of a *Drosophila* knock-out model and patient-derived fibroblasts suggests that mutations in this new ataxia/spasticity gene impact on mitochondrial structure and function.

This article is protected by copyright. All rights reserved.

Author Manuscript

Methods:

Patients:

Patients were identified in five different centers with a focus on movement disorders located in Case Western Reserve University (Ohio, US and genetically analyzed in Ann Arbor [Michigan, USA, UM1~~)~~]), Nijmegen and Rotterdam (The Netherlands, NIJ1-4), Lübeck (Germany, LUB1) and Winston-Salem (North Carolina, USA, WF1). Diagnostic testing (including gene panel analysis of known ataxia/spasticity genes) did not reveal a molecular diagnosis in these cases. All patients and relatives gave written informed consent to participate in diagnostic or research studies that were approved by the respective local IRBs (IRBMED University of Michigan, University of Lübeck ethics review panel, or to local (NIJ and Rotterdam) or commercial (WF1, GeneDx, Gaithersburg, MD) clinical exome sequencing (NIJ and WF1). Formation of this collaboration was facilitated by publication of grants funded by the National Ataxia Foundation and by "GeneMatcher".[8]

Genetic studies: Linkage analysis and exome sequencing

In Family UM1, linkage analysis was performed with DNA from all 5 affecteds, the mother and 7 unaffected siblings using the Infinium HumanLinkage-24 Beadchip kit (6000 markers, Illumina, WG-32-140), followed by parametric fully penetrant recessive model analysis in Merlin.[9]

In all families, whole exome sequencing was performed by exome capture [UM1: SeqCap EZ Exome v3.0 kit (Roche, CA, USA) at UM core facility; LUB1: ~~with~~ NexteraRapid Exome Capture kit (Illumina, Inc., San Diego, CA, USA) at Centogene (Rostock, Germany); all NIJ cases: SureSelectXT Human All Exon 50Mb Kit V5 (Agilent, CA, USA) at BGI Copenhagen, and WF1 at GeneDx (Gaithersburg, MD, USA)] followed by next generation sequencing on Illumina arrays (UM1 and LUB1: paired end HiSeq2000; LUB1 NextSeq500), to medium coverage of 46X (UM1), and ~75X (all NIJ, LUB1, and WF1).

This article is protected by copyright. All rights reserved.

Author Manuscript

For UM1, two cases were sequenced and variant analysis was restricted to the ~10 Mb linkage region. For LUB1, WF1 and NIJ4, parents were also sequenced and initially, a trio analysis for *de novo* variants (no damaging hits) was performed. Variants were called as follows: UM1.1 and UM1.4: Alignment was done using BWA against Human 1K Genome reference, duplicates were removed using Picard (v1.74), base recalibration, realignment and variant calling were done using GATK (v3.3); these samples were part of a 734-sample pooled call; LUB1: Variant calling was performed as described;[10] NIJ: Clinical exome sequencing and variant calling as described.[11] WF1: GeneDx clinical whole exome pipeline. Detected variants were filtered for rare (European population frequency <0.01) and protein-changing variants under a recessive model. VPS13D variants emerged as the strongest candidate in all cases.

All *VPS13D* variants were Sanger confirmed and segregation in the family consistent with compound heterozygosity was verified.

Copy number variant analysis was not performed on all samples. Since single exonic deletions are hard to detect in whole exome analyses, they hence can't be ruled out. Since all patients were compound heterozygous, a whole gene deletion in *VPS13D* can be ruled out.

Analysis of expression: ~~Splice site prediction, quantitative RT-PCR~~, ~~and~~ Nonsense-mediated decay and splice site prediction

~~In addition to nonsense and missense mutations, we detected three variants at splice sites (c.941+3A>G, c.2237-1G>C, c.9998+4A>C). Since it was not possible (including ethical reasons that do not allow to skin biopsy children) to get skin samples from these patients, we used two online slicing site prediction tools to estimate the impact of these variants on splicing: Human Splicing Finder (HSF, http://www.umd.be/HSF3/)[12] and Splice Site Prediction, set to mammals (SSP,~~

This article is protected by copyright. All rights reserved.

Author Manuscript

~~http://www.fruitfly.org/seq_tools/splice.html). HSF provides a consensus value (CV) variation as output with the interpretation of CV < 10% indicating a disruption of the splice site. SSP generates a score between 0 and 1 with a score of 0.5 recognizing about 90% of the actual sites and a false positive rate of <5%. The higher the score, the higher the probability that the splice site is active.~~

Since *VPS13D* expression is higher ~~expressed~~ in skin (fibroblasts) than in blood, we used mRNA extracted from a fibroblast culture to study expression levels and nonsense-mediated mRNA decay in Family UM1 (data not shown) and Patient LUB1.1. ~~For Family UM1, RNA was extracted using a Zymogen column (DNA digested in the column using DNase), and reverse transcribed using SuperSriptIII (Invitrogen 18080044). Primers to amplify a cDNA fragment containing both familial mutations in exon 20 were placed into the adjacent exons: VPS13Dex19F, agctacactgaacgaccgat and VPS13Dex21R, acacgagattgtccagggtt. RT-PCR products were Sanger-sequenced.~~ For Patient LUB1.1, RNA was extracted using the QIAmp RNA Extraction Kit (QIAGEN, Germantown, MD, USA). Oligo-dT-Nucleotides of the Maxima First Strand cDNA Synthesis Kit (ThermoFisher, Waltham, MA, USA) served as primers to synthesize the complementary DNA (cDNA) by use of reverse transcriptase (RT). PCR was performed with primers in Exons 21 and 22 (VPS13Dex21F: TGATTCCTTAGTCCACATCAAC, VPS13Dex22R: ATCATTTCCAGGTGTGCTAC) and the respective product was inspected for its size and Sanger sequenced. Further, the expression of VPS13D in LUB1.1 and a control was compared to the expression of *ß-Actin* and *HPRT*, and *YAZ* that served as reference genes. These quantitative PCRs were performed with SYBR Green on the LightCycler 480 system (data not shown). Since both qPCR and sequencing indicated instability of the allele with the nonsense mutation, we treated fibroblasts of LUB1.1 with cycloheximide for 8 hours at 100µg/ml final concentration to stabilize the transcript and confirm nonsense-mediated mRNA decay (NMD) as cause. Effect of cycloheximide was evaluated by sequencing of cDNA).

In addition to nonsense and missense mutations, we detected three variants at splice sites

This article is protected by copyright. All rights reserved.

Author Manuscript

(c.941+3A>G, c.2237-1G>C, c.9998+4A>C). Since we are limited to perform skin biopsy for research purposes in adults only, per our IRB, we do not have fibroblast cultures from the children with splice mutations~~Since our consent forms are designed to limit skin biopsy to adults, we do not have fibroblast cultures from the patients with splice mutations~~. Instead ~~it was not possible (including ethical reasons that do not allow to skin biopsy children) to get skin samples from these patients.~~ we used two online slicing site prediction tools to estimate the impact of these variants on splicing: Human Splicing Finder (HSF, http://www.umd.be/HSF3/)[12] and Splice Site Prediction, set to mammals (SSP, http://www.fruitfly.org/seq_tools/splice.html). HSF provides a consensus value (CV) variation as output with the interpretation of CV <-10% indicating a disruption of the splice site. SSP generates a score between 0 and 1 with a score of 0.5 recognizing about 90% of the actual sites and a false-positive rate of <5%. The higher the score, the higher the probability that the splice site is active.

Formatted: Indent: First line: 0"

Comparison of mutation frequencies in *VPS13D* paralogs

To assess the impact of the loss of function of each *VPS13* paralogs, we compared phenotypes of animal models available in the literature and in databases, and examined estimates of mutation frequencies in humans. To assess the common mutation types (e.g. loss of function, missense) in each *VPS13* paralog-associated disease, we restricted analysis to cases in which both mutations are known.

Functional studies in ~~human cells including~~ patient-derived fibroblasts

From the UM1 family, we established fibroblast cell lines from two patients (UM1.2 and UM1.4) and two controls (UM1.17, a daughter of an affected, and UMCtrl1, a married-in unaffected spouse). From LUB1, fibroblast lines were established from LUB1.1, the index patient, and her heterozygous parents (LUB1.3 and LUB1.4). In addition, fibroblasts from two unrelated control lines, LUBCtrl1, aka L-2132, and LUBCtrl2, aka L-2134, were used.

This article is protected by copyright. All rights reserved.

Author Manuscript

For mitochondrial imaging in fibroblast from the UM1 family, MitoTracker Red CMXRos (Invitrogen) was applied to fibroblasts cultured on coverslips for 40 minutes before fixing in 4% paraformaldehyde for 12 minutes. Through PLAPON 60X (1.42 Oil) lens on Olympus FV1000 confocal microscope, 6-8 z-stacks of images were obtained per visual field to produce images of in total 72 ~ 127 cells per line. Images were flattened using z-projection at maximum intensity using the open software Fiji,[13] which was also used to generate intensity histograms. For each 2-D image, the Otsu algorithm was applied to extract the top 1% brightest pixels. To quantify spherical mitochondria, any areas smaller than 1.5 μm^2 and with less circularity than 0.18 were removed using Fiji's Analyze Particles function. The remaining selected areas correspond to bright and spherical mitochondria. The average number of such selected objects per cell was calculated in each cell line. We also computed the percentage of cells with >2 such objects in the perinuclear region. Form factor analysis as a measurement of the mitochondrial network integrity was performed by using a selection algorithm in the software program Volocity (Perkin Elmer) to select mitochondrial objects (1 standard deviation above the mean MitoTracker intensity) of a projected Z-stack image (average intensity). For each projected image containing 4-12 cells, form factor defined as $[P_m^2]/[4\pi A_m]$ with P_m being the perimeter and A_m being the area of a mitochondrion, was calculated for all selected mitochondria and the mean was obtained for the entire image field. For each individual, 11-17 images from two independent experiments were analyzed.

In fibroblasts of Family LUB1, the form factor was determined as previously described.[14] In brief, the mitochondrial network in fibroblasts was stained with an anti-GRP75 antibody (1: 1000, Abcam, Cambridge, MA) in combination with the the Zenon immunolabelling kit (Invitrogen, Carlsbad, CA) according to manufacturer's protocol. Based on single cell images, mitochondria area and outline were measured and the form factor was calculated. Mean form factor was averaged over 20 cells per individual.

This article is protected by copyright. All rights reserved.

Author Manuscript

Measurement of the rate of ATP synthesis in cultured fibroblasts

ATP was quantified, in triplicate, using the ATP Bioluminiscence Assay Kit CLS II (Roche Diagnostics), following manufacture's instruction. ATP is measured in a luminometer (Berthold, Detection System), and calculated as ATP generated (µMoles) per minute per mg of protein. The amount of protein was determined using the BCA protein Assay Kit (Pierce).

Functional studies in *Drosophila* models

All fly lines and related constructs were purchased from the Bloomington Stock Center, including Vps13D mutant lines [#56282 ($Vps13D^{11101}$) and 22996, only #56282 homozygous shown], Vps13D RNAi (#38320), motoneuron-specific Gal4 driver (D42-Gal4, #8816), a deficiency line Df(3L)Exel6117 (#7596), as well as fluorescent mitochondrial marker (UAS-mitoGFP, #42727).[15] All phenotypes observed of homozygous Vps13D mutant alleles were confirmed in compound heterozygous flies of the two alleles, and in mutant alleles over the deficiency line, which lacks a defined region of the *Drosophila* chromosome containing the entire Vps13D genetic locus and some neighboring genes. For staining, we used the following primary antibodies: ATP5A (Abcam ab14748), 1: 1000 GFP (Life Technologies A-11122, 1:1000), Horse Radish Peroxidase (HRP) (Jackson 123-605-021,1:1000), DLG (DSHB 4f3, 1:1000). All secondary antibodies were from Invitrogen (Alexa-conjugated 1:1000, 2 hrs, RT). Standard dissection and immunostaining procedures were used for larval tissue analysis.[16] For larval immunostaining, tissues were fixed with 4% formaldehyde for 20 minutes at room temperature prior to staining, except for anti-ATP5A staining in which tissue was fixed with Bouin's Fixative for 7 minutes at room temperature. Form factor analysis of larval ventral nerve cords was performed using Volocity to select mitochondrial networks in the cell bodies of RNAi expressing motoneurons based on threshold of mitoGFP fluorescence (2.5 standard deviations above the mean fluorescence intensity) from a projected Z-stack image. For each cell body, an average form factor of all mitochondria was calculated.

This article is protected by copyright. All rights reserved.

Author Manuscript

Statistical analyses

Differences were analyzed statistically using unpaired t-tests, or analysis of variance (ANOVA) with a Bonferroni-Dunn post-hoc correction.

This article is protected by copyright. All rights reserved.

Author Manuscript

Results

Genetic Findings

Overview: In four different locations in the US and Europe, we independently detected compound heterozygous *VPS13D* mutations in 7 families. The mutational spectrum included five nonsense, five missense, one frameshift, one essential and two nonessential splice site mutations (~~Fig~~Table~~.~~ 2). All families carried a combination of one loss-of-function mutation (LOF: nonsense, frameshift, or essential splice sites) and one presumably milder change (missense or nonessential splice site mutation)~~.~~. All variants were absent or extremely rare (<13 heterozygous carriers) in the ~120,000 individuals listed in GnomAD. Among the five missense mutations, Gly1190Asp and Met1307Ile found in families UM1 and NIJ1 were located in the center of the protein. The three C-terminal missense mutations detected in families LUB1, NIJ2 and NIJ3 are close to or within the C-domain (Fig~~.~~ 1D~~2~~), which is conserved and unique among all VPS13 proteins including yeast.

UM1 ataxia family (SCAR4): We have previously reported a family with 14 siblings, five of whom with adult-onset spinocerebellar ataxia with saccadic eye intrusion (Fig 1A, *SCAR4* [6, 7]). After exclusion of known ataxia mutations, genome-wide linkage analysis under a recessive, full penetrance model identified only a single locus with LOD > 0, which was 20 cM/ ~10 Mb on chromosome 1p36 flanked by rs7538691 and rs761162 (LOD = 3.1, data not shown). Whole exome sequencing in two affected individuals revealed compound heterozygous mutations in *VPS13D* as the only likely genetic cause within the linked region. The ~~changes~~ variants comprised a paternally inherited missense change (c.3569G>A, p.Gly1190Asp) and a maternally inherited stop-gain ~~variant~~ mutation (c.3316C>T, p.Gln1106Ter). Sanger sequencing verified segregation among all 12 siblings with available DNA samples. Sequencing of RT-PCR products from fibroblast cell lines of two patients demonstrated that the stop-gain allele-containing mRNA product was less abundant, suggesting that it underwent nonsense-mediated decay (data not shown). pGly1190Asp introduces an extra negative charge and

This article is protected by copyright. All rights reserved.

Author Manuscript

appears not to affect protein stability (data not shown).

Family LUB1: In two affected sisters of a German family with spastic ataxia (Fig 1B), we detected compound heterozygous mutations in *VPS13D* including a maternal nonsense mutation (Tyr1803Ter) and a paternal missense change (Ala4210Val, rs746736545). Similar to Family UM1, sequencing of cDNA of the index patient revealed the allele with the nonsense mutation to be less abundant. Treatment with cycloheximide stabilized the mutated allele and confirmed that the nonsense-mutated allele indeed underwent NMD (Fig. 1C). NMD resulted in a decreased expression level of about 50-60% in Patient LUB1.1 (data not shown).

Additional sporadic cases: At the Radboudumc expert centre for genetic movement disorders in Nijmegen, and the genetic movement clinic in Rotterdam, the Netherlands, four unrelated cases of different ethnicities with compound heterozygous *VPS13D* mutations were independently identified (Table 1). NIJ1 and NIJ2 carry a combination of a nonsense mutation and a missense change, NIJ3 a frameshift and a non-essential splice site mutation, and NIJ4 carries an essential splice site mutation and a missense change (Figure Table 2). NIJ4 also has optic atrophy and carries a heterozygous frameshift mutation in *OPA1* [c.1156_1157del (p.Leu386Glufs*2)]. A second (biallelic) mutation in *OPA1* was excluded by exome sequencing with sufficient coverage of the entire coding region and splice sites. Her mother carried the same variant and has isolated optic atrophy.

At the Wake Forest School of Medicine, Winston-Salem, North Carolina, USA, one additional case, WF1, was identified by clinical exome sequencing (GeneDx, Gaithersburg, MD). WF1 displayed hypotonia, balance and coordinating difficulties, as well as global developmental delay; more formal clinical ataxia tests were difficult to perform, due to her current age and disease features as well as global developmental delay. WF1 has a combination of a nonsense mutation and nonessential splice site change.

This article is protected by copyright. All rights reserved.

Author Manuscript

To estimate the impact of the splice site changes on the transcript, we used two different *in-silico* splice site prediction programs. As expected, both programs, HSF and SSP, strongly predicted an effect on splicing of the invariant acceptor splice site of intron 18 in NIJ4, c.2237-1G>C (Fig 2), which hence was classified LOF. The splice region variants in NIJ3 and WF1, however, are not within invariant splice consensus sites. For c.9998+4>C in intron 49, CV variation was -10.57%, thus just below HSF's -10 cut-off. SSP's prediction score dropped from 0.93 to 0.62 suggesting ~~an~~ a mild, if any, impact on recognition of this splice site. For c.941+3A>G in intron 9, the CV variation was -0.83% by the HSF algorithm and would argue against an effect on splicing. However, the SSP score dropped from 0.89 to 0.21, suggesting reduction in predicted splicing ability. These two non-essential splice site mutations are hence not considered complete LOF alleles as they may allow some correctly spliced transcripts. Confirmatory analysis of intronic ~~splicing~~splice region variants could not be performed at this time (~~refer~~see ~~to the~~ m~~M~~ethods for details).

Clinical findings

All cases except for WF1, which was too young, had either ataxia or spasticity as a core symptom. Onset ranged from infancy to early adulthood. The UM1 family, previously assigned *SCAR4*, demonstrated primarily adult-onset ataxia with distinct macrosaccadic intrusions[7], with pyramidal features, neuropathy, and myoclonus but no intellectual disability[6]. Videos of the clinical exams and the distinct eye phenotype are available in the online supplement of that reference[7]. The two sisters from family LUB1 were in their onset and clinical phenotypes similar to UM1, except for a different oculomotor phenotype. By contrast, NIJ1 had a much earlier onset (< 5 yrs) and symptoms were more debilitating (wheelchair-bound by age 17 yrs). Whether his phenotypic difference originates from more severe *VPS13D* mutations or other environmental or genetic factors is unknown at this time. Similarly, NIJ4 and WF1 were severely affected with an age at onset in the first year of life. In addition to ataxia and neuropathy, NIJ4 suffers from developmental delay, seizures, and optic atrophy. Coincidentally, she carries an additional mutation in *OPA1 (Optic Atrophy 1/ Mitochondrial Dynamin Like GTPase)*

This article is protected by copyright. All rights reserved.

Author Manuscript

which explains the optic atrophy but not the additional seizures and the developmental delay. NIJ2 was affected by spastic paraplegia without ataxia, with onset in early adulthood. Patients WF1 and NIJ3 might be more severely affected due to two severe mutations including a non-essential splice site change and a LOF mutation, in contrast to the combination of a missense and a LOF mutation in the other subjects.

Among *VPS13* paralogs, *VPS13D* is the most intolerant to mutations

Yeast *vps13* is implicated in many cellular functions including sporulation, Golgi organization, and mitochondrial integrity.[18] During metazoan evolution, two duplication events gave rise to three paralogs–*VPS13A/C, B, and D*. *Drosophila* Vps13 (CG2093) is an ortholog of *VPS13A/C,* which further duplicated in the vertebrate evolution into *VPS13A* and *VPS13C* (updated from reference [19]). Since not much is known about *VPS13D*-specific function, we compared reported phenotypes of VPS13 homologs in the two model organisms fly and mouse [fly database CG2093 [20], mouse: MGI2444304 [21], MGI2444207, and MGI2448530] (Table ~~2~~3). Mutations in *Vps13D*/*VPS13D* cause embryonic lethality in both animals, while mutations in *VPS13A and C* appear more tolerable during early development (animal phenotypes for *VPS13B* are unavailable).

A similar trend was observed in human populations (Table ~~2~~3): RVIS (Residual Variation Intolerance Score) is a gene-based intolerance score derived from allele frequency in whole exome sequence data.[22] Among the paralogs, *VPS13D* has the lowest RVIS score of -4.23, 0.14 percentile, suggesting *VPS13D* is among the most mutation-intolerant of human genes. We also compared the frequency of LOF in each paralog in the ExAC (Exome Aggregation Consortium) browser. Again, *VPS13D* emerges as most sensitive to LOF mutations, with the lowest ratio of the number of variants observed over expected. For *VPS13D*, the probability of LOF intolerance, pLI score, is 1, virtually certain. Indeed, chorea acanthocytosis is caused in 29/31 cases by LOF/LOF mutations in *VPS13A,*[23] Cohen syndrome in 41/45 cases by LOF/LOF mutations in *VPS13B,* [24-28] and Parkinson's disease in 3/4 cases by LOF/LOF mutations in *VPS13C* cases.[29, 30] In summary, *VPS13D* is intolerant to complete LOF of both

This article is protected by copyright. All rights reserved.

Author Manuscript

alleles, being likely incompatible with life, consistent with our finding of only compound heterozygous missense/LOF or nonessential splice/LOF mutations.

***Vps13D* disruption in *Drosophila* is lethal and causes mitochondrial defects**

Known also as CG32113 in flies, fly Vps13D shows 33% protein identity to the human gene (Table ~~2~~3). Consistent with *Vps13d* lethality in mice, flies disrupted for *Vps13D* do not survive beyond 2nd instar larvae stage. This lethality was confirmed with two independent lines containing large insertions in the coding region of *Vps13D*, including compound heterozygous animals containing one copy of each *Vps13D* allele, hence ruling out secondary mutations as the cause of lethality.

Since the only yeast vps13 protein has previously been implicated in mitochondrial function,[29] we hypothesized that loss of *Drosophila* Vps13D may alter mitochondria. In early 2nd instar larvae before lethality, we observed that deletion of *Vps13D* led to severe alterations in mitochondrial morphology. Instead of forming fine mitochondrial networks in individual cells, mitochondria appear as singular, enlarged objects. This abnormal mitochondrial appearance was present in the larval brain (Fig ~~3A~~2A) and other tissues in these young larvae (not shown). By contrast, no differences were detected for cellular markers of other organelles (Golgi, ER, lysosomes and the nucleus; data not shown).

We then used RNAi-mediated knockdown[31] to inhibit expression of *Vps13D* specifically in motoneurons. This allows for survival of larvae to the 3rd instar stage (death at pupal stage), which enables further characterization of Vps13D's autonomous function in neurons. By co-expression of mitoGFP targeted specifically to mitochondria of the RNAi depleted neurons,[15] we observed enlarged spherical mitochondria (Fig ~~3B~~2B). Compared to a control RNAi line targeting luciferase, knockdown by Vps13D RNAi resulted in a significant reduction in quantified form factor (Fig ~~3C~~2C), consistent with a loss of complexity of the mitochondria network coinciding with enlarged, isolated mitochondria. These observations suggest a role for Vps13D in regulating mitochondrial morphology and potentially also mitochondrial function in neurons.

The abnormal mitochondrial network in neuronal cell~~s~~ bodies led us to hypothesize that loss of

This article is protected by copyright. All rights reserved.

Author Manuscript

Vps13D would deleteriously impact the distribution of mitochondria to distal regions of neurons.

Previous studies have linked deficiencies in mitochondrial trafficking to distal neurites in neurodegenerative diseases and neuropathies.[32, 33] We observed that reduction of Vps13D in motoneurons led to strong impairment in the distribution of mitochondria in peripheral axons in segmental nerves (Fig 4A3A, B) and neuromuscular junction (NMJ) synapses (Fig 4C3C, D). The density of mitochondria was progressively reduced concomitant with increased distance from the cell body locations in the CNS (Fig 43). This failure to distribute mitochondria resembles previously described defects for mutations in mitochondrial fission/fusion machinery.[32]

Patient-derived fibroblasts show altered mitochondrial morphology

Given these fly data, we also investigated mitochondrial function and morphology in human fibroblasts. Staining fibroblasts from the affected subjects of family UM1 with MitoTracker, which accumulates in mitochondria in a membrane potential dependent manner, revealed significantly brighter mitochondria (Fig 54). While the typical mitochondrial network of elongated objects and branches was observed in both control and patient cells, the perinuclear regions of only affected cells often contained unusually bright and significantly more spherical mitochondrial objects, which were mostly in clusters and at higher magnification appeared to be donut-shaped (Fig 5G4G). To quantify the abundance of the bright and spherical mitochondria in each cell line, we extracted the top 1% brightest pixels from each image and selected circular objects based on computed circularity score. The average number of such abnormal mitochondrial objects was ~ 6-fold higher in the affected compared to control cells (Fig 5H4H). In the perinuclear region, such objects were identified in clusters (≥ 3) in ~10% of normal but 91% and 67% of fibroblasts of affected subjects' cells (Fig 5I4I). Consistent with the *Drosophila* data, form factor analysis also revealed a significant reduction in the degree of mitochondrial branching in the affected fibroblasts compared to controls (Fig 5J4J). These observations suggest structural defects in mitochondria in VPS13D-deficient fibroblasts.

This article is protected by copyright. All rights reserved.

Author Manuscript

Independent analysis of fibroblasts of the proband of family LUB1 demonstrated that the affected fibroblasts expressed reduced levels of mitochondrial GRP75 protein compared to controls (Fig ~~6~~ 5A-C). Form factor analysis of GRP75 immunostaining revealed a similar reduction in the degree of mitochondrial branching of proband fibroblasts compared to two unrelated healthy controls (Fig ~~6D~~5D). These structural mitochondrial changes were accompanied by a reduced ATP production rate of LUB1.1 compared to control fibroblasts (Fig ~~6E~~5E).

Discussion

In this study, we have identified seven different compound heterozygous mutations in *VPS13D* in twelve patients and link VPS13D/Vps13D defects in patient fibroblasts and in flies to mitochondrial deficits. Our study also included a large family with ataxia (*SCAR4*) and linkage to a 10-Mb region on chromosome 1p36 including the *VPS13D* gene.

The core phenotype of the eleven patients above the age of 2 with compound heterozygous *VPS13D* mutations is characterized by movement disorders of the ataxia-spasticity spectrum, ranging from predominant ataxia, spastic ataxia, to spastic paraplegia without ataxia, and ataxia plus phenotypes. The latter included two cases with an additional developmental delay phenotype (NIJ3 and NIJ4). The youngest patient, WF1 of age 2 at the last evaluation~~,~~ ~~, too young to be formally diagnosed with ataxia,~~ presented with ~~ severe gait difficulties,~~ presented with hypotonia and developmental delay, including motor delay, ~~and hypotonia~~ and was~~ere~~ not yet ambulatory ~~yet~~. These three patients also have different types or additional mutations, as NIJ3 and WF1 carry nonessential splice region ~~mutations~~ variants in addition to an LOF. This may be more severe than the combination of missense/LOF found in the other cases. In addition, NIJ4's presentation may be complicated by an additional mutation in *OPA1*. The protein encoded by *OPA1* is also implicated in mitochondrial function. It is conceivable that there ~~is~~ may be an interactive effect of the two mutations linked to mitochondrial dysfunction. ~~This may result in the severe phenotype in patient NIJ4 due to digenic inheritance, but we cannot be certain based on just a~~

This article is protected by copyright. All rights reserved.

Author Manuscript

~~single case.~~ Interestingly, recent data have shown that about 5% of patients carry two independent Mendelian diseases.[34] ~~.~~ However, digenic inheritance can't be ascertained based on this single case. Of note, homozygous or compound heterozygous *OPA1* mutations cause an extended multi-system phenotype that includes ataxia and spastic paraplegia, known as Behr syndrome.[17] ~~.~~ While there was complete coverage of the *OPA1* coding regions and splice sites, no second mutation in the *OPA1* gene was detected by exome nor by copy number analyses (conducted as described)[35] ~~)~~. Hence, although we cannot exclude an undetected intronic or promoter mutation that is not penetrant, as the father does not have optic atrophy, we believe Behr syndrome as an alternative diagnosis ~~of~~ in this case is ~~ruled out~~not likely. ~~.~~

The overlap between genetic forms of ataxias and hereditary spastic paraplegias is well recognized, as there are other examples of genes (e.g., *SPG7*) that when mutated can give rise to either pure ataxia or spastic paraplegia or to a mixed phenotype of spastic ataxia,[36, 37] ~~and~~ developmental delay, and seizures, and other complex phenotypes commonly accompany early onset recessive ataxias.[2] In addition, there was variability in age of onset in our patients, which is also not unusual for ataxias. Frequently observed neurological co-morbidities in our series included peripheral axonal neuropathy and extrapyramidal signs such as myoclonus and dystonia. Infertility was noted in two male cases. Although it is currently uncertain whether this is *VPS13D*-related, infertility is a known feature of mitochondrial disease.[38]

VPS13D encodes a large protein (4388 amino acids), whose paralogs cause other neurological disorders: *VPS13A* mutations cause chorea acanthocytosis, characterized by a severe hyperkinetic movement disorder, myopathy, epileptic seizures, cognitive decline and behavioral changes,[23, 39] and perturb protein homeostasis in the fly.[20] *VPS13B* is involved in Cohen syndrome[40, 41] and *VPS13C* in rare cases of genetic Parkinson's disease with mitochondrial dysregulation and mitophagy.[29] ~~.~~ Most of these disease-associated mutations are LOF/LOF (see Table ~~2~~3). In contrast to the other VPS13

This article is protected by copyright. All rights reserved.

Author Manuscript

paralogs, knocking out *VPS13D's* homologs in *Drosophila* (our results) and mouse (MGI:2448530) leads to embryonic lethality, and not a single LOF/LOF mutation was identified, suggesting that some residual VPS13D function in humans may be critical for survival. In addition, the ExAC server's pLI score, i.e. the probability that a gene may be intolerant to haploinsufficiency, for *VPS13D* is 1, in contrast to all other *VPS13* genes (Table ~~2~~3). [42]~~.~~ We did not, however, observe the predicted intolerance to haploinsufficiency, as one parent of each of the cases reported here was haploinsufficient, but none were symptomatic, including one parent who lived into their 90s without apparent neurological problems.

Our genetic data allow for some first, yet cautious speculations on genotype-phenotype correlations. First, our current data collectively point to missense/LOF mutations tending to cause relatively pure ataxia and/or spasticity. Second, as suggested by the more severe NIJ3 and WF1 cases, who carry non-essential splice site/LOF mutations, other mutation type combinations may be associated with a broader and/or more severe spectrum of phenotypes. Lastly, the other severe case, NIJ4, had a co-existent dominant *OPA1* mutation and corresponding optic atrophy,[43] which was also observed in the subject's mother. The *OPA1* mutation may contribute epistatically to the phenotype since *OPA1* also affects mitochondrial function.[43]

Although our study convincingly establishes missense/LOF mutations in *VPS13D* as causing ataxia/spastic paraplegia and mitochondrial pathology, many questions remain to be addressed. Clinically, predicting the phenotype from new mutations in *VPS13D* will be difficult. Even for missense/LOF mutation carriers, the clinical presentation varied in our series. In addition, homozygous or compound heterozygous missense mutations were not observed here. As *VPS13D* is a large gene with many missense variants reported in databases including homozygosity,[42] it will be even more difficult to predict pathogenicity of any novel biallelic missense variants.

This article is protected by copyright. All rights reserved.

Manuscript

While further work is warranted to pin down the precise mitochondrial defect, we have shown abnormal mitochondrial morphology in both flies and patient cell lines, and reduced mitochondrial function in fibroblasts. Mitochondrial dysfunction is associated with several other ataxias and spastic paraplegias such as Friedreich's ataxia,[44] *SCA28*,[45] *POLG*,[46] and *SPG7*,[47] as well as in some unexplained ataxias.[48] Although we observed a defect in mitochondrial distribution in both *Drosophila* neurons lacking Vps13D and patient fibroblasts containing mutations in *VPS13D*, the precise biological underpinnings of this defect are still under investigation, including electron microscopy studies to assess mitochondrial morphology. Alterations of mitochondrial dynamics such as transport, fission, and/or fusion[32] can all potentially manifest in aberrant distribution of mitochondria throughout the cell. Various mutations in mitochondrial genes lead to the production of reactive oxygen species,[49] which can additionally disrupt mitochondrial distribution in neurons. Combining the *in vitro* cellular model of patient fibroblasts and neurons differentiated from induces pluripotent stem cells with *in vivo* experiments in the genetic fly model may help us parse out the cellular role of VPS13D in mitochondrial biology and disease progression. These methods will also allow for testing of potential therapies that target mitochondrial dysfunction and that could be common to other forms of ataxia and spastic paraplegias.

While this manuscript was under review, Anding et al. published findings showing VPS13D to be a ubiquitin-binding protein and affecting mitochondrial fission and fusion,[50] consistent with our findings, and also implemented VPS13D in autophagy, a process that we have recently reported to be involved in ataxia.[51]

Acknowledgment

We thank the patients for their willingness to participate and patience during our research. We thank Dr. Philipp Capetian for clinical evaluation of Family LUB1 and referring to the study. Linda Gates, Thomas Kubisiak, and Frauke Hinrichs for excellent technical assistance; Johann Gudjonsson, MD

Author

This article is protected by copyright. All rights reserved.

Author Manuscript

(Dermatology, University of Michigan) for fibroblast biopsies, Soochin Cho (Creighton University) for useful discussion on VPS13 evolution; Bart Post, MD, PhD and Jolanda Schieving, MD (Department of Neurology, Radboud university medical centre, Nijmegen, the Netherlands) and M. Jongen, MD, PhD (Department of Neurology, Erasmus MC, Rotterdam, the Netherlands) and Aasef Shaikh, MD (Neurology, Case Western Reserve) for providing important clinical data.

This work was supported by the US National Institutes of Health grants NS056780 (MB), NS069844 (CC), and F32NS098611 (RI), the National Ataxia Foundation (MB), European Union's Horizon 2020 research innovation program under the ERA-NET Cofund action N° 643578, ZonMW (9003037604; BvdW) under the frame of the E-Rare-3 network PREPARE, the Hersenstichting (BvdW), Radboud university medical centre (BvdW) and Bioblast Pharma (BvdW), the Foundation of the University Hospital Schleswig-Holstein ("Gutes Tun!", AM), and a career development award from the Hermann and Lilly Schilling Foundation (CK).

Author Contributions:

JZL, AM, VS, CK, CC, KL, BvdW, MB contributed to the conception and design of the study

ESe, RI, MD, E-JK, JT, NB, ESa, SL, ABO, TJ, AJAK contributed to acquisition and analysis of data

ESe, RI, MD, E-JK, CK, CC, KL, BvdW, MB contributed to drafting the text and preparing the figures

Potential Conflicts of Interests:

None of the authors report COI relevant to the reported work. See disclosures for other detailed COI

This article is protected by copyright. All rights reserved.

Author Manuscript

Literature Cited

1. Sandford E, Burmeister M. Genes and genetic testing in hereditary ataxias. Genes (Basel). 2014;5(3):586-603.

2. Beaudin M, Klein CJ, Rouleau GA, Dupre N. Systematic review of autosomal recessive ataxias and proposal for a classification. Cerebellum Ataxias. 2017;4:3.

3. Marras C, Lang A, van de Warrenburg BP, et al. Nomenclature of genetic movement disorders: Recommendations of the International Parkinson and Movement Disorder Society task force. Mov Disord. 2017 May;32(5):724-5.

4. Fogel BL, Lee H, Deignan JL, et al. Exome sequencing in the clinical diagnosis of sporadic or familial cerebellar ataxia. JAMA Neurol. 2014 Oct;71(10):1237-46.

5. Synofzik M, Schule R. Overcoming the divide between ataxias and spastic paraplegias: Shared phenotypes, genes, and pathways. Mov Disord. 2017 Mar;32(3):332-45.

6. Swartz BE, Burmeister M, Somers JT, Rottach KG, Bespalova IN, Leigh RJ. A form of inherited cerebellar ataxia with saccadic intrusions, increased saccadic speed, sensory neuropathy, and myoclonus. Ann N Y Acad Sci. 2002 Apr;956:441-4.

7. Swartz BE, Li S, Bespalova I, et al. Pathogenesis of clinical signs in recessive ataxia with saccadic intrusions. Ann Neurol. 2003 Dec;54(6):824-8.

8. Sobreira N, Schiettecatte F, Valle D, Hamosh A. GeneMatcher: a matching tool for connecting investigators with an interest in the same gene. Hum Mutat. 2015 Oct;36(10):928-30.

9. Abecasis GR, Cherny SS, Cookson WO, Cardon LR. Merlin--rapid analysis of dense genetic maps using sparse gene flow trees. Nat Genet. 2002 Jan;30(1):97-101.

10. Trujillano D, Bertoli-Avella AM, Kumar Kandaswamy K, et al. Clinical exome sequencing: results from 2819 samples reflecting 1000 families. Eur J Hum Genet. 2017 Feb;25(2):176-82.

11. van de Warrenburg BP, Schouten MI, de Bot ST, et al. Clinical exome sequencing for cerebellar ataxia and spastic paraplegia uncovers novel gene-disease associations and unanticipated rare disorders. Eur J Hum Genet. 2016 Oct;24(10):1460-6.

This article is protected by copyright. All rights reserved.

Author Manuscript

12. Desmet FO, Hamroun D, Lalande M, Collod-Beroud G, Claustres M, Beroud C. Human Splicing Finder: an online bioinformatics tool to predict splicing signals. Nucleic Acids Res. 2009 May;37(9):e67.

13. Schindelin J, Arganda-Carreras I, Frise E, et al. Fiji: an open-source platform for biological-image analysis. Nat Methods. 2012 Jun 28;9(7):676-82.

14. Grunewald A, Voges L, Rakovic A, et al. Mutant Parkin impairs mitochondrial function and morphology in human fibroblasts. PLoS One. 2010 Sep 27;5(9):e12962.

15. Pilling AD, Horiuchi D, Lively CM, Saxton WM. Kinesin-1 and Dynein are the primary motors for fast transport of mitochondria in Drosophila motor axons. Mol Biol Cell. 2006 Apr;17(4):2057-68.

16. Klinedinst S, Wang X, Xiong X, Haenfler JM, Collins CA. Independent pathways downstream of the Wnd/DLK MAPKKK regulate synaptic structure, axonal transport, and injury signaling. J Neurosci. 2013 Jul 31;33(31):12764-78.

17. Carelli V, Sabatelli M, Carrozzo R, et al. 'Behr syndrome' with OPA1 compound heterozygote mutations. Brain. 2015 Jan;138(Pt 1):e321.

18. Myers MD, Payne GS. Vps13 and Cdc31/centrin: Puzzling partners in membrane traffic. J Cell Biol. 2017 Feb;216(2):299-301.

19. Velayos-Baeza A, Vettori A, Copley RR, Dobson-Stone C, Monaco AP. Analysis of the human VPS13 gene family. Genomics. 2004 Sep;84(3):536-49.

20. Vonk JJ, Yeshaw WM, Pinto F, et al. Drosophila Vps13 Is Required for Protein Homeostasis in the Brain. PLoS One. 2017;12(1):e0170106.

21. Tomemori Y, Ichiba M, Kusumoto A, et al. A gene-targeted mouse model for chorea-acanthocytosis. J Neurochem. 2005 Feb;92(4):759-66.

22. Petrovski S, Gussow AB, Wang Q, et al. The Intolerance of Regulatory Sequence to Genetic Variation Predicts Gene Dosage Sensitivity. PLoS Genet. 2015 Sep;11(9):e1005492.

23. Dobson-Stone C, Velayos-Baeza A, Jansen A, et al. Identification of a VPS13A founder mutation in French Canadian families with chorea-acanthocytosis. Neurogenetics. 2005 Sep;6(3):151-8.

This article is protected by copyright. All rights reserved.

Author Manuscript

24. Hennies HC, Rauch A, Seifert W, et al. Allelic heterogeneity in the COH1 gene explains clinical variability in Cohen syndrome. Am J Hum Genet. 2004 Jul;75(1):138-45.

25. Katzaki E, Pescucci C, Uliana V, et al. Clinical and molecular characterization of Italian patients affected by Cohen syndrome. J Hum Genet. 2007;52(12):1011-7.

26. Kolehmainen J, Wilkinson R, Lehesjoki AE, et al. Delineation of Cohen syndrome following a large-scale genotype-phenotype screen. Am J Hum Genet. 2004 Jul;75(1):122-7.

27. Seifert W, Holder-Espinasse M, Kuhnisch J, et al. Expanded mutational spectrum in Cohen syndrome, tissue expression, and transcript variants of COH1. Hum Mutat. 2009 Feb;30(2):E404-20.

28. Seifert W, Holder-Espinasse M, Spranger S, et al. Mutational spectrum of COH1 and clinical heterogeneity in Cohen syndrome. J Med Genet. 2006 May;43(5):e22.

29. Lesage S, Drouet V, Majounie E, et al. Loss of VPS13C Function in Autosomal-Recessive Parkinsonism Causes Mitochondrial Dysfunction and Increases PINK1/Parkin-Dependent Mitophagy. Am J Hum Genet. 2016 Mar 3;98(3):500-13.

30. Schormair B, Kemlink D, Mollenhauer B, et al. Diagnostic exome sequencing in early-onset Parkinson's disease confirms VPS13C as a rare cause of autosomal-recessive Parkinson's disease. Clin Genet. 2017 Sep 01.

31. Dietzl G, Chen D, Schnorrer F, et al. A genome-wide transgenic RNAi library for conditional gene inactivation in Drosophila. Nature. 2007 Jul 12;448(7150):151-6.

32. Baloh RH. Mitochondrial dynamics and peripheral neuropathy. Neuroscientist. 2008 Feb;14(1):12-8.

33. Yu Y, Lee HC, Chen KC, et al. Inner membrane fusion mediates spatial distribution of axonal mitochondria. Sci Rep. 2016 Jan 08;6:18981.

34. Posey JE, Harel T, Liu P, et al. Resolution of Disease Phenotypes Resulting from Multilocus Genomic Variation. N Engl J Med. 2017 Jan 5;376(1):21-31.

35. Pfundt R, Del Rosario M, Vissers L, et al. Detection of clinically relevant copy-number variants by exome sequencing in a large cohort of genetic disorders. Genet Med. 2017 Jun;19(6):667-75.

This article is protected by copyright. All rights reserved.

Author Manuscript

36. de Bot ST, Willemsen MA, Vermeer S, Kremer HP, van de Warrenburg BP. Reviewing the genetic causes of spastic-ataxias. Neurology. 2012 Oct 02;79(14):1507-14.

37. van Gassen KL, van der Heijden CD, de Bot ST, et al. Genotype-phenotype correlations in spastic paraplegia type 7: a study in a large Dutch cohort. Brain. 2012 Oct;135(Pt 10):2994-3004.

38. Demain LA, Conway GS, Newman WG. Genetics of mitochondrial dysfunction and infertility. Clin Genet. 2017 Feb;91(2):199-207.

39. Tomiyasu A, Nakamura M, Ichiba M, et al. Novel pathogenic mutations and copy number variations in the VPS13A gene in patients with chorea-acanthocytosis. Am J Med Genet B Neuropsychiatr Genet. 2011 Jul;156B(5):620-31.

40. Balikova I, Lehesjoki AE, de Ravel TJ, et al. Deletions in the VPS13B (COH1) gene as a cause of Cohen syndrome. Hum Mutat. 2009 Sep;30(9):E845-54.

41. Megarbane A, Slim R, Nurnberg G, Ebermann I, Nurnberg P, Bolz HJ. A novel VPS13B mutation in two brothers with Cohen syndrome, cutis verticis gyrata and sensorineural deafness. Eur J Hum Genet. 2009 Aug;17(8):1076-9.

42. Exome Aggregation Consortium (ExAC). Cambridge, MA2015 [updated 2015/01/16/]; Available from: http://exac.broadinstitute.org.

43. Chun BY, Rizzo JF, 3rd. Dominant optic atrophy: updates on the pathophysiology and clinical manifestations of the optic atrophy 1 mutation. Curr Opin Ophthalmol. 2016 Nov;27(6):475-80.

44. Jasoliya MJ, McMackin MZ, Henderson CK, Perlman SL, Cortopassi GA. Frataxin Deficiency Impairs Mitochondrial Biogenesis in Cells, Mice and Humans. Hum Mol Genet. 2017 Apr 21.

45. Pierson TM, Adams D, Bonn F, et al. Whole-exome sequencing identifies homozygous AFG3L2 mutations in a spastic ataxia-neuropathy syndrome linked to mitochondrial m-AAA proteases. PLoS Genet. 2011 Oct;7(10):e1002325.

46. Finsterer J. Ataxias with autosomal, X-chromosomal or maternal inheritance. Can J Neurol Sci. 2009 Jul;36(4):409-28.

This article is protected by copyright. All rights reserved.

Author Manuscript

47. Shanmughapriya S, Rajan S, Hoffman NE, et al. SPG7 Is an Essential and Conserved Component of the Mitochondrial Permeability Transition Pore. Mol Cell. 2015 Oct 01;60(1):47-62.

48. Bargiela D, Shanmugarajah P, Lo C, et al. Mitochondrial pathology in progressive cerebellar ataxia. Cerebellum Ataxias. 2015;2:16.

49. Hayashi G, Cortopassi G. Oxidative stress in inherited mitochondrial diseases. Free Radic Biol Med. 2015 Nov;88(Pt A):10-7.

50. Anding AL, Wang C, Chang TK, et al. Vps13D Encodes a Ubiquitin-Binding Protein that Is Required for the Regulation of Mitochondrial Size and Clearance. Curr Biol. 2017 Dec 30.

51. Kim M, Sandford E, Gatica D, et al. Mutation in ATG5 reduces autophagy and leads to ataxia with developmental delay. Elife. 2016 Jan 26;5.

This article is protected by copyright. All rights reserved.

Author Manuscript

Figure Legends:

Figure 1. Multiplex ataxia families with compound heterozygous mutations in *VPS13D*

A. Pedigree of Family UM1 ~~family~~. Affected siblings are indicated by black filled symbols while unaffected individuals are marked by unfilled symbols. The nine unaffected siblings are shown in an open diamond. Mutational status is given below each individual together with the respective laboratory ID. **B.** Pedigree of Family LUB1 with mutations in the two affected sisters, shown by black filled symbols. **C.** cDNA sequences of the c.5409C>A mutation before (top panel) and after (lower panel) treatment with cycloheximide. The traces are representative of N2 ~~number of~~sequencing runs. The nonsense-mutated allele got stabilized and showed similar expression levels upon treatment. **BD.** Predicted domain maps of VPS13D protein (http://www.ebi.ac.uk/interpro/protein/Q5THJ4) with the identified missense mutations marked: N1: VPS13 1st N-terminal domain (aa 2-115), N2: VPS13 2nd N-terminal domain (aa 137-356), U: UBA (Ubiquitin-associated)-like domain (aa 2627-2679), SHR: VPS13 SHORT ROOT transcription factor-binding domain (aa 3276-3558), C: VPS13 C-terminal domain (aa 3983-4129). The five different missense mutations appear to cluster in two regions, one ~~of them the C-terminal domain~~in the middle and the other near the C domain. **CE**. Amino acid sequence alignments of the regions surrounding each missense mutation across various species. While Gly1190Asp, Asn4107Ile, and Gly4149Ser are conserved in all VPS13D orthologs, Met1307Leu and Ala4210Val are conserved in mammals and chicken but not in zebrafish and/or fruitfly.

Formatted: Highlight

This article is protected by copyright. All rights reserved.

Author Manuscript

Figure 2. Overview of mutations in *VPS13D* identified in ataxia/spasticity cases

A. Coordinates of all detected mutations (GRCH37/hg19 built, NM_015378), respective *in silico* prediction (CADD score and MutationTaster), frequency in public exome/genome databases (GnomAD: genome aggregation consortium at http://gnomad.broadinstitute.org/gene/ENSG00000048707), and splice site prediction scores by Human Splicing Finder (http://www.umd.be/HSF3/) and Splice Site Prediction (http://www.fruitfly.org/seq_tools/splice.html) **B.** Predicted domain maps of VPS13D protein (http://www.ebi.ac.uk/interpro/protein/Q5THJ4) with the identified missense mutations marked: N1: VPS13 1st N-terminal domain (aa 2-115), N2: VPS13 2nd N-terminal domain (aa 137-356), U: UBA (Ubiquitin-associated)-like domain (aa 2627-2679), SHR: VPS13 SHORT ROOT transcription factor-binding domain (aa 3276-3558), C: VPS13 C-terminal domain (aa 3983-4129). The five different missense mutations appear to cluster in two regions, one of them the C-terminal domain. **C.** Amino acid sequence alignments of the regions surrounding each missense mutation across various species. While Gly1190Asp, Asn4107Ile, and Gly4149Ser are conserved in all VPS13D orthologs, Met1307Leu and Ala4210Val are conserved in mammals and chicken but not in zebrafish and/or fruitfly.

This article is protected by copyright. All rights reserved.

Author Manuscript

Figure ~~3~~2. Disruption of *Vps13D* in the *Drosophila* central nervous system affects mitochondrial morphology.
A. Ventral nerve cord (VNC), stained for mitochondrial marker ATP5A, of control (w^{1118}, right panel) and *Vps13D* mutant ($Vps13D^{11101/11101}$, left panel) *Drosophila* larvae. Bottom: High magnification single confocal Z-planes of areas indicated by the dashed boxes, highlighting mitochondrial morphology in neuronal cell bodies. Scale Bars: 50µm (top) and 5µm (bottom) **B**. Representative images of motoneurons (via D42-Gal4) with simultaneous expression of fluorescent mitochondrial marker mitoGFP (green) along with control (left panel) and *Vps13D* (right panel) RNAi expression. Bottom: High magnification single confocal Z-planes of areas indicated by the dashed boxes, highlighting mitochondrial morphology in motoneuron cell bodies. **C.** Quantification of form factor analysis of the mitochondrial network (based on mitoGFP) in neuronal cells bodies expressing control RNAi (white) vs. *Vps13D* RNAi (grey). n=50 neurons per condition (from 5 different animals). Error bars represent standard error. *** indicates $p<0.001$ (Students T-test).

Formatted: Line spacing: single, Widow/Orphan control, Adjust space between Latin and Asian text, Adjust space between Asian text and numbers, Tab stops: Not at 0.5" + 1" + 1.5" + 2" + 2.5" + 3"

This article is protected by copyright. All rights reserved.

Author Manuscript

Figure 43: Knockdown of *Vps13D* in *Drosophila* motoneurons disrupts the distribution of mitochondria to distal ~~regions of neurons~~axons.

A. Segmental nerves (HRP, red) containing motoneuron axons expressing fluorescent mitochondrial marker mitoGFP (green) of control RNAi and Vps13D RNAi knock~~ed~~ down (RNAi) animals. Nerves near the VNC (proximal, top) and distant from the VNC (distal, bottom) are shown. Scale Bar: 10μm. **B**. Quantification of the mitochondrial content per area within segmental nerves in proximal and distal regions of motoneurons expressing control RNAi (white) vs. *Vps13D* RNAi (grey). Data is normalized to Control RNAi Proximal Region condition. n≥10 individual nerves from 5 different animals. Error bars represent standard error. **** indicates p<0.0001 (Students T-test). **C**. Larval NMJ synapses from motoneuron axons expressing fluorescent mitochondrial marker mitoGFP (green) of control and Vps13D RNAi knock~~ed~~ down animals. HRP (red) labels neuronal membrane, while DLG (blue) labels NMJ postsynaptic region. High magnification images of the synaptic region (indicated by the dashed box) are shown (right panels) to highlight mitochondria occupying the synaptic region. Scale Bar: 20μm (left) and 2.5μm (right). **D**. Quantification of the mitochondrial content in the NMJ synapse per area of motoneurons expressing control RNAi (white) vs. *Vps13D* RNAi (grey). Data is normalized to Control RNAi condition. n=5 animals (each n represents the avg. mitochondrial content of ≥6 NMJ synapses/animal). Error bars represent standard error. **** indicates p<0.0001 (Students T-test).

This article is protected by copyright. All rights reserved.

Author Manuscript

Figure ~~5~~4. Patient fibroblasts contain abnormal spherical mitochondria

A-D: Comparison of mitochondria in 4 fibroblast lines of Family UM1 ~~family~~ stained with MitoTracker: A, UMCtrl1: wild type for *VPS13D*; B, UM1.17: asymptomatic heterozygous carrier of the Gly1190Asp missense mutation; C and D, UM1.2 and UM1.4: VPS13D compound heterozygous patients. Note that while the majority of the mitochondria in the control cells are elongated and of similar intensity, the patient cells are loaded with particularly bright, circular mitochondrial objects mostly localized in perinuclear region. **E**: Intensity histogram of MitoTracker images. The X-axis represents the intensity, the numbers of pixels are plotted on the Y-axis (the black plots in natural number scale and the gray plot in log-scale). Note that both patients have many more pixels with higher intensity, indicative of the increase in bright MitoTracker-stained objects. **F** and **G**: Perinuclear mitochondria at higher magnification (60X lens, 4X zoom). Control mitochondria (F, UMCtrl1) are elongated, tubular, and interconnected while the patient mitochondria (G, UM1.2) are often donut-shaped. Here, brightness was individually optimized to reveal the structural details and is not comparable. Scale Bars: 20 µm (A-D) and 2 µm (F and G). **H**: Average number of circular mitochondria (MT) objects identified by image processing. Such circular objects are present in the control cell lines at low frequencies but become much more abundant in the affected cell lines (~6-fold increase). **I**: Percentage of cells with at least 3 perinuclear circular MT objects. The patient fibroblast cultures have higher number of cells with perinuclear circular MT objects than control (6- and 9-fold increase). **J.** Form factor analysis of the mitochondrial network stained by MitoTracker. In H to J, error bars represent standard error. *, **, and *** indicate $p<10^{-4}$, $p<10^{-5}$, and $p<10^{-6}$ respectively (Student's T-test).

This article is protected by copyright. All rights reserved.

Author Manuscript

Figure ~~6~~5. Altered mitochondrial morphology and decreased ATP in *VPS13D* mutant fibroblasts. **A.** Western blot analysis shows mitochondrial GRP75 protein levels in the *VPS13D*-mutant fibroblasts (LUB1.1), patient's parents (LUB1.3 and LUB1.4), and healthy control fibroblasts (LUBCtrl2) with β-actin as loading control. **B.** Quantification of the above GRP75 Western blot using ImageJ. **C.** The mitochondrial network was investigated under basal conditions by confocal microscopy in fixed cells immunostained with anti-GRP75. Scale Bar: 20 µm. **D.** Form factor as a measure for mitochondrial interconnectivity (GRP75 immunostaining) was calculated for two control fibroblast lines (LUBCtrl1, LUBCrtl2) and one patient line (LUB1.1) (n=20). Each dot represents measurement in a single cell. The mean values, and the standard deviations of the investigated individuals are shown. **E.** ATP production was determined based on luminescence. ATP concentration (µmoles) was calculated per minute per milligram of protein (n=3 independent experiments). In B and E, the error bars indicate SEM of n≥3 independent experiments.

This article is protected by copyright. All rights reserved.

Table 1. Clinical presentations of each ataxia case with VPS13D mutations identified

	UM1.1-5	LUB1.1-2	NIJ1	NIJ2	NIJ3	NIJ4	WF1
Mutation	p.Gln1106* p.Gly1190Asp	p.Tyr1803* p.Ala4210Val	p.Gln662* p.Met1307Leu	p.Gln2572* p.Gly4149Ser	p.Val2987Glyfs*14 c.941+3A>G	c.2237-1G>C p.Asn4107Ile	p.Leu2277* c.9998+4A>C
Sex	M; M; F; M; M	F; F	M	F	M	F	F
Origin	Slovenian	German	Dutch	Javanese	Dutch	Dutch	Lumbee/German/ Scottish
Age at last evaluation	54; 52; 50; 49; 47	35; 29	43	29	37	6	2
Onset age	39; 36; 28; 23; 34	29; 20	<5	28	<3-4	<1	<1
Presenting symptom	Gait (1-4) and reading (1-5) difficulties	Gait (1,2) and speech (2) difficulties	Delayed walking, spastic gait	Gait difficulties	Delayed walking, abnormal gait	Developmental delay	Delayed gross motor skills
Core phenotype	Cerebellar ataxia	Spastic ataxia	Spastic ataxia	Spastic paraplegia	Spastic ataxia	Ataxia and neuropathy	Hypotonia
Mobility	Wheelchair (1,3); Walker (2,4); Independent (5)	Independent (1); Wheelchair (2)	Wheelchair	Independent	Wheelchair	Independent	Not walking
Cerebellar signs	+	+	+	-	+	-	+
Oculomotor	Horizontal saccadic oscillations	Saccadic pursuit, SWJ, hypermetric vertical saccades (1); NA (2)	SWJ	-	Jerky pursuit, slow hypermetric saccades	Gaze-evoked nystagmus	NA
Dysarthria	+	- (1); + (2)	-	-	+	+	NA
UL ataxia	+	+	+	-	+	+	NA
LL ataxia	+	+	NA	-	+	+	NA
Gait ataxia	+	+	NA	-	+ (stance)	+	nonambulatory secondary to balance/coordi-nation difficulties
Pyramidal signs	+	+	+	+	+	-	-
UL spasticity	NA	- (1); NA (2)	-	-	-	-	-
LL spasticity	NA	+	-	+	+	-	-
Spastic gait	-	+	NA	+	NA	-	NA
Plantar response	Extensor	Extensor (1); NA (2)	Extensor	Equivocal to extensor	Extensor	Equivocal	Flexor
Tendon reflexes	Increase at knees, decrease at ankles	Increased UL/ LL (1); NA (2)	Increased UL/ LL	Increased LL	Absent ankle jerks, rest increased	Areflexia	Increased UL/ LL
Weakness/ atrophy	Mild calf atrophy (1-4); None (5)	Moderate LL (1); NA (2)	Severe LL	Mild LL	Severe LL	Mild proximal/ distal UL and LL	None
Seizures	-	-	-	-	-	+	-
Cognitive state	Normal	Mild executive dysfunction (1); Normal (2)	Normal	Normal	Normal	Mild ID	Speech delayed
Extrapyramidal signs	Myoclonus	-	-	-	Cervical dystonia	-	-
Sensory exam	Impaired joint position sense	Reduced deep sensory functions LL (1); NA (2)	Deep sensory loss distal LL	Normal	Sensory loss distal LL	NA	Normal
Brain MRI	Mild cerebellar atrophy with dorsal vermis involvement	Normal (1); NA (2)	Signal changes in corticospinal tract	Normal	Atrophy /hypoplasia cerebellar vermis inferior; subtle white matter changes centrum semiovale	Cerebellar atrophy	Normal
NCS/EMG	Mild to moderate sensorimotor axonal neuropathy	Normal (1); NA (2)	Normal	NA	NA	Axonal neuropathy	NA
Additional information		SEP:LL prolonged latencies & MEP: increased cortical latencies (1); Deterioration due to pregnancies (2)	Macrocephaly Oligospermia		Azoospermia	Optic atrophy OPA1 mutation: c.1156_1157del, p.Leu386Glufs*2	Poor eye contact; frequent hand flapping and head banging

M: male, F: female, UL: upper and LL: lower limb, +: present, -: absent, NA: no assessment, SWJ: square wave jerks, ID: intellectual disability; NCS/EMG: nerve conduction studies, electromyography; MEP: magnetic evoked potential; SEP: sensory evoked potential. In columns 2 and 3, patient sexes and ages are given in id order (1-5 in UM1, 1-2 in LUB1), which are noted in parenthesis when phenotypes differ.

This article is protected by copyright. All rights reserved.

Author Manuscript

Author Manuscript

	Mutation Protein NP_056193	Mutation cDNA NM_015378	Mutation Genomic level	CADD score	Mutation Taster	Frequency GnomAD	Human Splicing Finder	Splice Site Prediction
UM1	Gly1190Asp	3569G>A	chr1:12337214G>A	25	Disease causing	Not reported		
	Gln1106Ter	3316C>T	chr1:12336961C>T	39	Disease causing	Not reported		
LUB1	Ala4210Val	12629C>T	chr1:12520418C>T	34	Disease causing	0.00004039		
	Tyr1803Ter	5409C>A	chr1:12343568C>A	33	Disease causing	Not reported		
NIJ1	Met1307Leu	3919A>T	chr1:12337564A>T	19	Disease causing	0.00004885		
	Gln662Ter	1984C>T	chr1:12331062C>T	40	Disease causing	Not reported		
NIJ2	Gly4149Ser	12445G>A	chr1:12516165G>A	35	Disease causing	Not reported		
	Gln2572Ter	7714C>T	chr1:12382602C>T	51	Disease causing	Not reported		
NIJ3	Splicing	941+3A>G	chr1:12317147A>G	17	NA	Not reported	-0.83%	0.89→0.21
	Val2987GlyfsX14	8960_8961delTG	chr1:12405505delTG	35	Disease causing	Not reported		
NIJ4	Asn4107Ile	12320A>T	chr1:12476867A>T	30	Disease causing	Not reported		
	Splicing (essential)	2237-1G>C	chr1:12335881G>C	23	NA	Not reported	-31.07%	0.99→0.00
WF1	Splicing	9998+4A>C	chr1:12416585A>C	9.6	NA	0.00003738	-10.57%	0.93→0.62
	Leu2277Ter	6829delC	chr1:12371876delC	35	Disease causing	Not reported		

Table 2. Compound heterozygous *VPS13D* mutations identified in each ataxia/spasticity family

Coordinates of all detected mutations are based on NM_015378 for cDNA and GRCH37/hg19 built for genomic DNA. CADD score and MutationTaster are *in-silico* prediction of deleteriousness of each mutation. 3 of the mutations have been reported previously in public exome/genome databases (gnomAD: genome aggregation consortium at http://gnomad.broadinstitute.org/gene/ENSG00000048707). For splice mutations, splice site prediction scores were calculated at Human Splicing Finder (http://www.umd.be/HSF3/) and Splice Site Prediction (http://www.fruitfly.org/seq_tools/splice.html).

This article is protected by copyright. All rights reserved.

Table 3. Mutations of *VPS13D* paralogs in animals and humans

Yeast Cellular functions implicated	**Fruit fly paralogs** mutant phenotypes	**Vertebral paralogs** Mouse null phenotypes	**Mutation Intolerance in human**				**Human disorder**		
			RVIS	**%ExAC v2 RVIS**	**LoF O/E**	**LoF pLI**	**Disorder**	**Disease mutation type**	
Vps13 [17] Sporulation, Integrity of mitochondria, Golgi organization, Organelle junction	***Vps13/ CG2093*** [19] Reduced life span, Neurodegene-ration	***VPS13A*** Viable, Acanthocytosis, Neurologically abnormal in 129/SvEv background [20]	-1.85 (2.03%)	-3.75 (0.51%)	30/ 119.0	0.00	Chorea acantho-cytosis [22]	1/31 1/31 29/31	MIS / MIS MIS / LOF+ LOF+ / LOF+
		VPS13C Viable, Neurologically normal #	-0.61 (17.5%)	-2.83 (1.20%)	83/ 141.1	0.00	Parkinson's disorder [28-29]	1/4 3/4	MIS / LOF LOF / LOF
	Vps13B/ CG15523 No data available	***VPS13B*** No data available	-0.81 (12.08%)	-2.13 (2.69%)	65/ 127.8	0.00	Cohen syndrome [23-27]	3/45 1/45 41/45	MIS / MIS MIS / LOF+ LOF+ / LOF+
	Vps13D/ CG32113 * Embryonic lethal, Mitochondrial defects	***VPS13D*** Embryonic lethal before placentation with complete penetrance $	-4.23 (0.14%)	-5.77 (0.11%)	28@/ 156.2	1.00	Ataxia *	5/7 2/7	MIS / LOF Splice? / LOF

RVIS: residual variation intolerance score (more negative more intolerant) with intolerance score ranked in all human genes given in paranthesis. %ExAC v2 RVIS: RVIS v4, constructed on ExAC v2 (gnomAD) release. LoF: Loss of function, stop-gained and essential splice site mutations. O/E: number of variants observed/expected. pLI: probability of LoF Intolerance (pLI >=0.9 regarded as extremely LoF intolerant). RVIS, LoF O/E and pLI are based on ExAC. @: For VPS13D, gnomAD lists 65 LoF variants, with no increased frequency in any particular geographic/ethnic population. MIS: missense. LOF: LoF plus frameshift. LOF+: In addition to LOF, large deletions/insertions included. #: MGI2444207. $: MGI2448530. *: This study

Author Manuscript

This article is protected by copyright. All rights reserved.

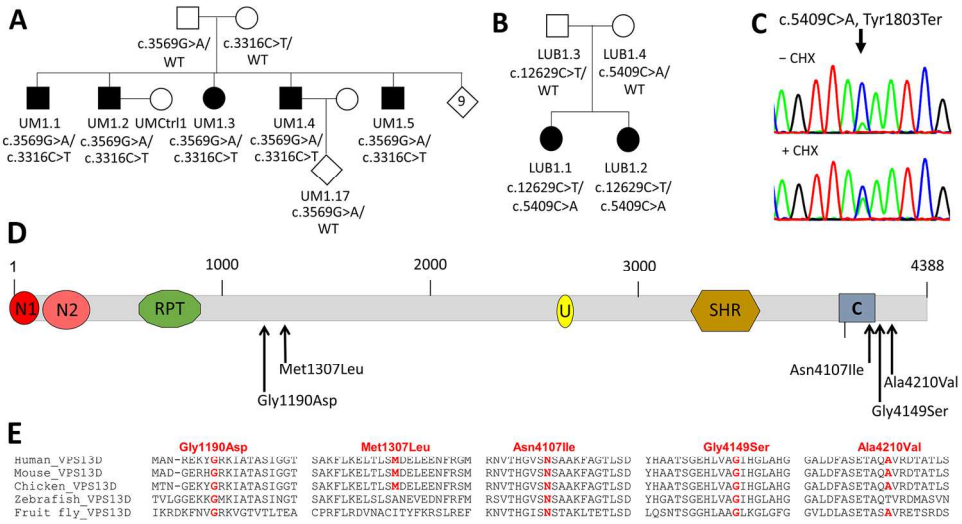

Figure 1: Multiplex ataxia families with compound heterozygous mutations in VPS13D

170x95mm (300 x 300 DPI)

Author Ma

This article is protected by copyright. All rights reserved.

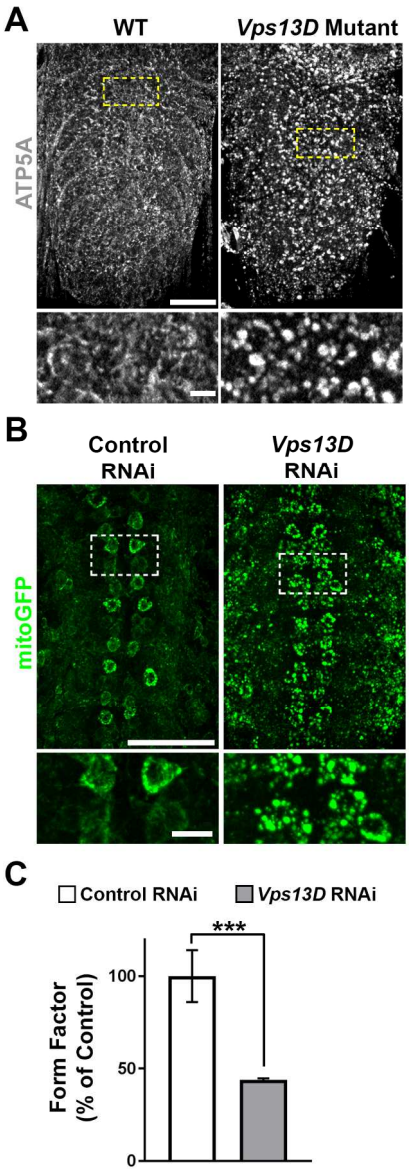

Figure 2: Disruption of Vps13D in the Drosophila central nervous system affects mitochondrial morphology.

80x225mm (300 x 300 DPI)

Au

This article is protected by copyright. All rights reserved.

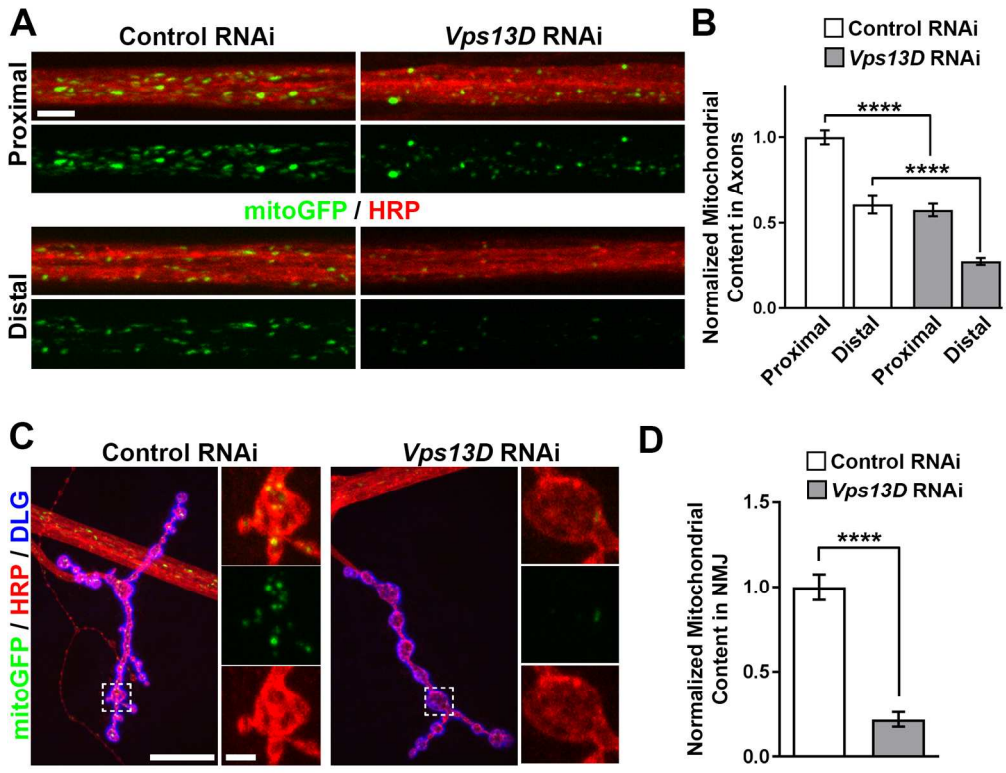

Figure 3: Knockdown of Vps13D in Drosophila motoneurons disrupts the distribution of mitochondria to distal axons

170x135mm (300 x 300 DPI)

Author

This article is protected by copyright. All rights reserved.

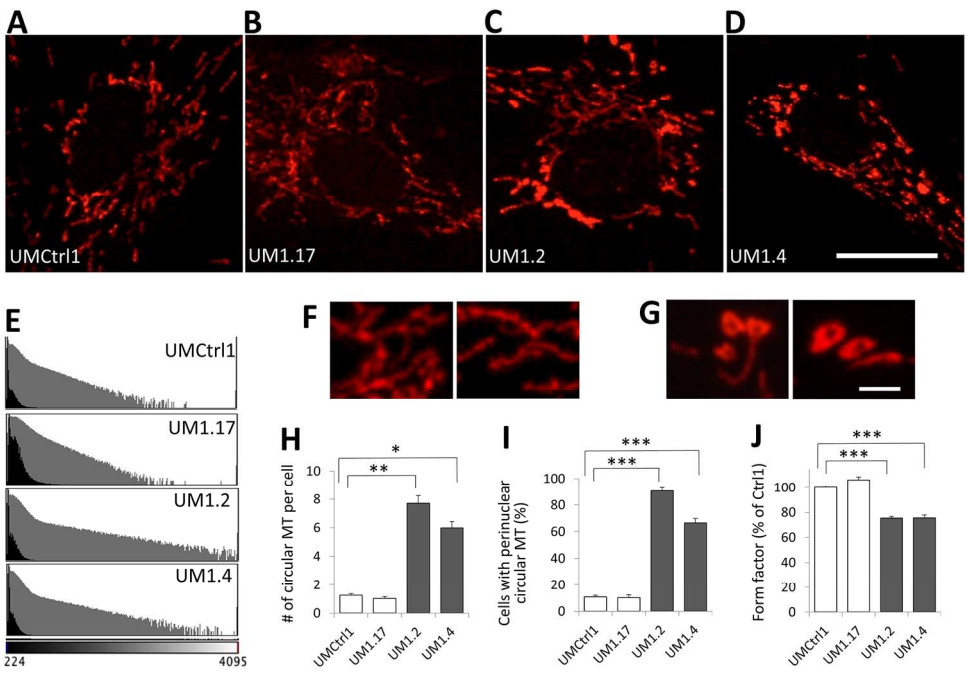

Figure 4: Patient fibroblasts contain abnormal spherical mitochondria

170x114mm (300 x 300 DPI)

Author M

This article is protected by copyright. All rights reserved.

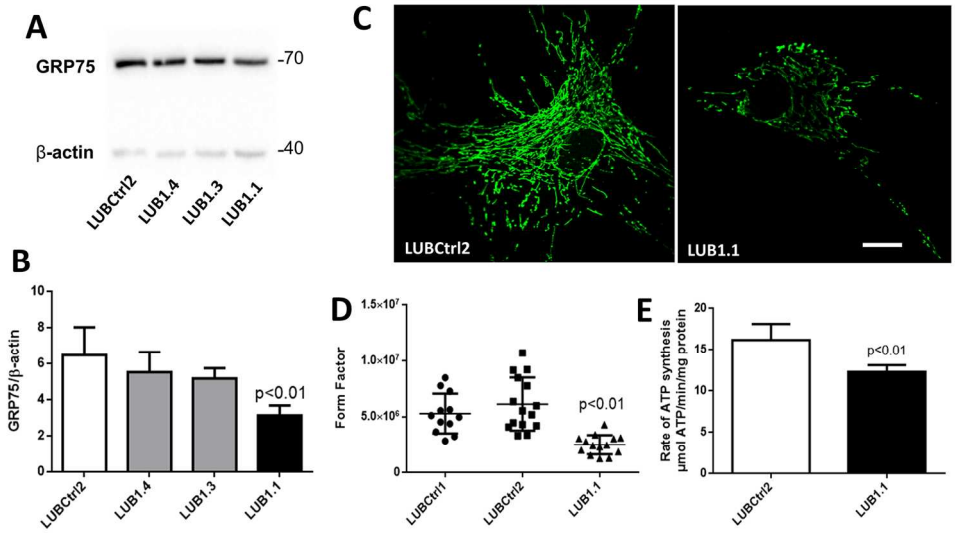

Figure 5: Altered mitochondrial morphology and decreased ATP in VPS13D mutant fibroblasts

170x93mm (300 x 300 DPI)

Author Ma

This article is protected by copyright. All rights reserved.

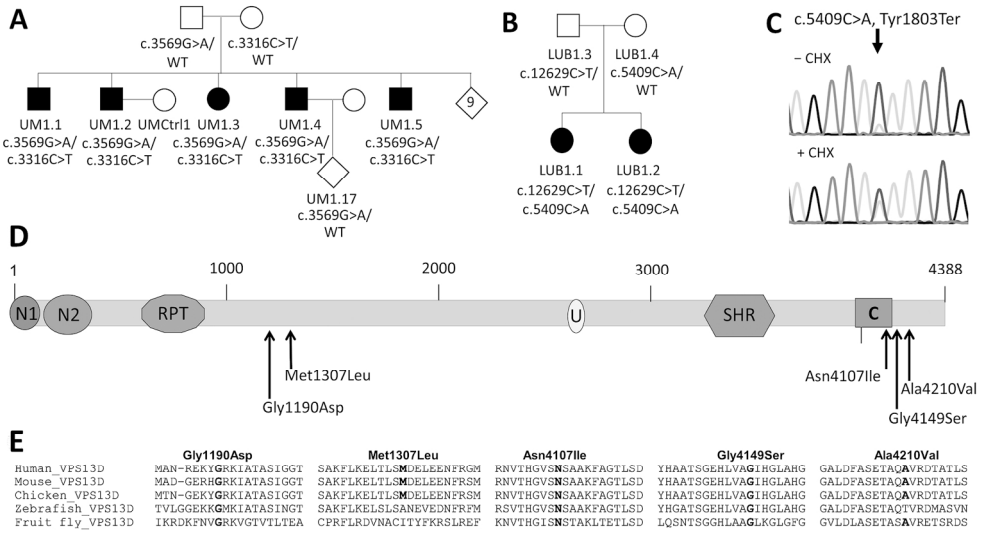

BW Figure 1: Multiplex ataxia families with compound heterozygous mutations in VPS13D

170x97mm (300 x 300 DPI)

Author Ma

This article is protected by copyright. All rights reserved.

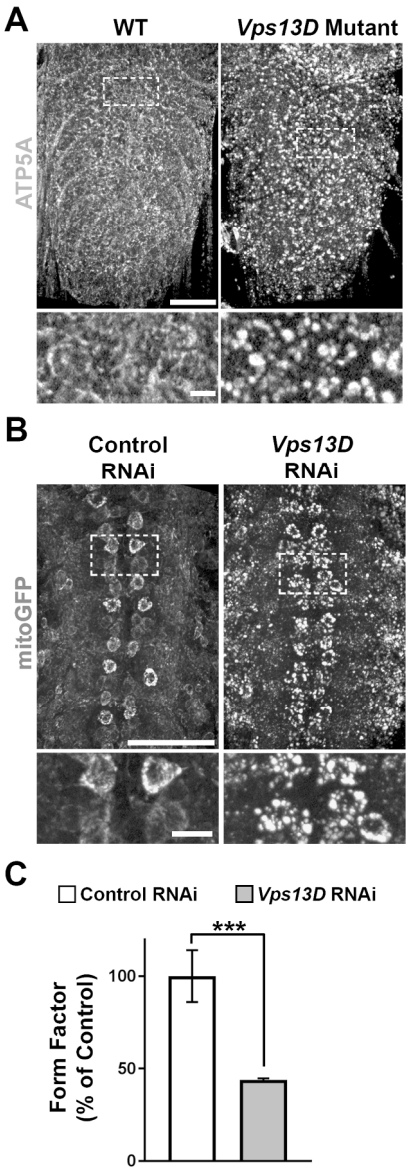

BW Figure 2: Disruption of Vps13D in the Drosophila central nervous system affects mitochondrial morphology

80x225mm (300 x 300 DPI)

Ac

This article is protected by copyright. All rights reserved.

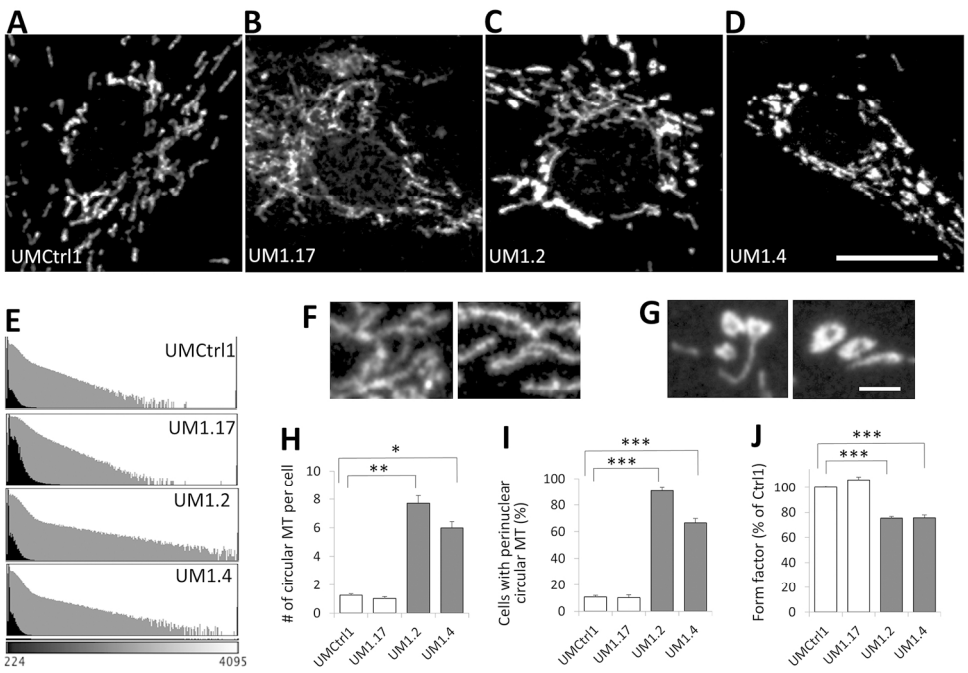

BW Figure 4: Patient fibroblasts contain abnormal spherical mitochondria

170x114mm (300 x 300 DPI)

Author M

This article is protected by copyright. All rights reserved.

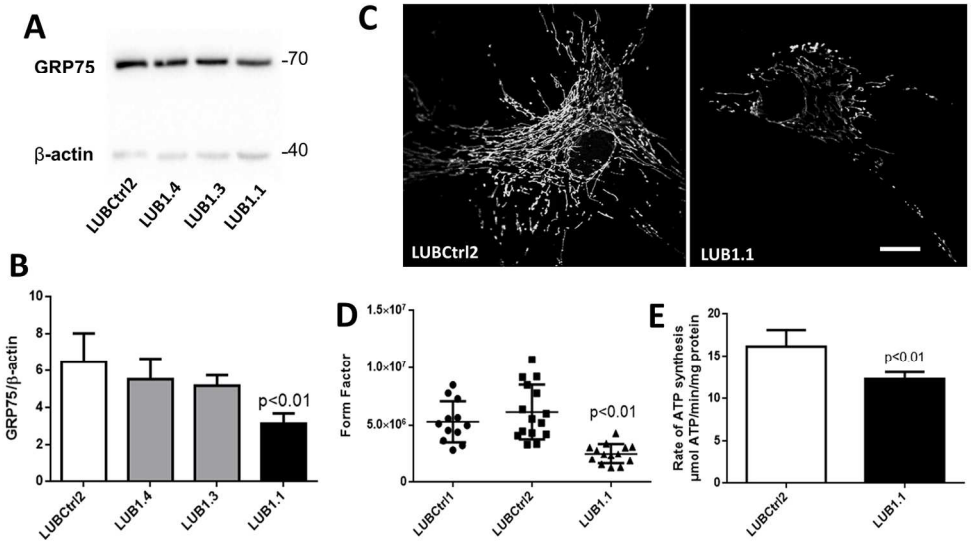

BW Figure 5: Altered mitochondrial morphology and decreased ATP in VPS13D mutant fibroblasts

170x97mm (300 x 300 DPI)

Author Ma

This article is protected by copyright. All rights reserved.